Molecular and Cellular Neuroscience 80 (2017) 1–17

Contents lists available at ScienceDirect

Molecular and Cellular Neuroscience

journal homepage: www.elsevier.com/locate/ymcne

NGF-dependent axon growth and regeneration are altered in sympathetic neurons of dystrophic *mdx* mice

Loredana Lombardi [a,1], Irene Persiconi [a,1], Alessandra Gallo [a], Casper C. Hoogenraad [c], Maria Egle De Stefano [a,b,*]

[a] Dipartimento di Biologia e Biotecnologie "Charles Darwin", Sapienza Università di Roma, Laboratory affiliated to Istituto Pasteur Italia – Fondazione Cenci Bolognetti, 00185 Roma, Italy
[b] Center for Research in Neurobiology "Daniel Bovet", Sapienza Università di Roma, 00185 Roma, Italy
[c] Cell Biology, Faculty of Science, Utrecht University, 3584CH Utrecht, The Netherlands

ARTICLE INFO

Article history:
Received 9 May 2016
Revised 9 December 2016
Accepted 29 January 2017
Available online 2 February 2017

Keywords:
Axon growth
Axon regeneration
Duchenne muscular dystrophy
Dystrophin-dystroglycan complex
mdx mice
NGF signaling
TrkA receptor

ABSTRACT

Duchenne muscular dystrophy (DMD) is a lethal disease, determined by lack of dystrophin (Dp427), a muscular cytoskeletal protein also expressed by selected neuronal populations. Consequently, besides muscular wasting, both human patients and DMD animal models suffer several neural disorders. In previous studies on the superior cervical ganglion (SCG) of wild type and dystrophic *mdx* mice (Lombardi et al. 2008), we hypothesized that Dp427 could play some role in NGF-dependent axonal growth, both during development and adulthood. To address this issue, we first analyzed axon regeneration potentials of SCG neurons of both genotypes after axotomy *in vivo*. While noradrenergic innervation of *mdx* mouse submandibular gland, main source of nerve growth factor (NGF), recovered similarly to wild type, iris innervation (muscular target) never did. We, therefore, evaluated whether dystrophic SCG neurons were poorly responsive to NGF, especially at low concentration. Following *in vitro* axotomy in the presence of either 10 or 50 ng/ml NGF, the number of regenerated axons in *mdx* mouse neuron cultures was indeed reduced, compared to wild type, at the lower concentration. Neurite growth parameters (*i.e.* number, length), growth cone dynamics and NGF/TrkA receptor signaling in differentiating neurons (not injured) were also significantly reduced when cultured with 10 ng/ml NGF, but also with higher NGF concentrations. In conclusion, we propose a role for Dp427 in NGF-dependent cytoskeletal dynamics associated to growth cone advancement, possibly through indirect stabilization of TrkA receptors. Considering NGF activity in nervous system development/remodeling, this aspect could concur in some of the described DMD-associated neural dysfunctions.

1. Introduction

Duchenne muscular dystrophy (DMD) is a common X -linked recessive disease, in which patients exhibit progressive and irreversible muscle degeneration, together with significant neurological abnormalities (Blake and Kroger, 2000; Mehler, 2000; Waite et al., 2009; Pilgram et al., 2010). The disease is caused by mutations in the DMD gene (Koenig et al., 1987), which encodes dystrophin, a protein of the cortical cytoskeleton of 427 kDa (Dp427) expressed in skeletal, cardiac and smooth muscles, in several brain areas (Mehler, 2000; Waite et al., 2009) and in autonomic neurons (De Stefano et al., 1997). Dp427 is part of a large trans-membrane glycoproteic complex, the dystrophin-associated glycoprotein complex (DGC), characterized by structural and signaling properties (Blake et al., 2002; Davies and Nowak, 2006). In contrast to the situation in muscles, where Dp427 expression reaches a plateau already in fetal life (Chelly et al., 1990), dystrophin expression in the brain appears to be developmentally regulated, possibly modulating aspects of neurogenesis, neuronal migration and differentiation, neuronal size and dendritic arborization (Jagadha and Becker, 1988; Mehler, 2000). Indeed, first major neuronal alterations in DMD patients and *mdx* mice, an animal model of the disease, occur during development, leading after birth to various degrees of cognitive and behavioral abnormalities (Pilgram et al., 2010; Anderson et al., 2002; Vaillend et al., 2004; Cyrulnik and Hintoon, 2008).

The peripheral nervous system (PNS) is also affected, as autonomic dysfunctions have been reported in DMD patients (Yotsukura et al., 1995). We previously described several structural and functional alterations in the superior cervical ganglion (SCG) of *mdx* mice, a sympathetic ganglion, which innervates different muscular (*i.e.* heart, iris) and non-muscular (*i.e.* salivary glands) targets and expresses Dp427 in wild type animals (De Stefano et al., 1997). In particular, between postnatal day 5 (P5) and 10 (P10), coinciding with the natural occurring cell death, the number of *mdx* mouse neurons projecting to muscular targets significantly decreased compared to wild type. However, well before the beginning of neuronal death (*i.e.* P0), noradrenergic innervation of muscular targets was also reduced, and all ganglionic neurons, regardless of the type of target they innervate, showed less axon

* Corresponding author at: Dipartimento di Biologia e Biotecnologie "Charles Darwin", Sapienza Università di Roma, Piazzale Aldo Moro 5, 00185 Roma, Italy.
E-mail address: egle.destefano@uniroma1.it (M.E. De Stefano).
[1] The first two authors equally contributed to this work.

http://dx.doi.org/10.1016/j.mcn.2017.01.006
1044-7431/

defasciculation and terminal branching (De Stefano et al., 2005; Lombardi et al., 2008). For these same post-natal dates, we also reported significant alterations in the protein levels of NGF receptors (TrkA and p75NTR), which suggested an imbalance in the NGF signaling cascade (Lombardi et al., 2008), and a differently modulated expression of genes encoding proteins involved in neuron survival and differentiation (Licursi et al., 2012).

Purpose of this study was to investigate the role of Dp427 in NGF-dependent axonal growth and regeneration, by using *in vivo* and *in vitro* experimental paradigms. Our results highlight a novel role for the Dp427-dystroglycan complex in axon growth of both maturing and regenerating neurons. This could be achieved by indirect stabilization of membrane-bound TrkA receptors and consequent mediation of the NGF-dependent cytoskeletal dynamics associated to growth cone advancement. These data could provide the incentive for new research aimed at developing therapeutic strategies to reduce neural dysfunctions and autonomic failures in DMD patients.

2. Materials and methods

2.1. Animals

Wild type and genetically dystrophic *mdx* C57BL/10 mice (The Jackson Laboratory, Bar Harbor, Maine, USA) were used. All studies were carried out in accordance with the guidelines promulgated in the National Institutes of Health Guide for the Care and Use of Laboratory Animals (NIH Guide, revised 1996), in the European Convention for the protection of Vertebrate Animals used for Experimental and Other Scientific Purposes of the Council of Europe (no. 123, June 15th, 2006), and in accordance with The Code of Ethics of the EU Directive 2010/63/EU. All efforts were made to minimize animal suffering, to reduce the number of animals used, and to utilize alternatives to *in vivo* techniques. The experimental procedures and protocols were approved by the Ethical Committee for Animal Research of the Italian Ministry of Public Health.

2.2. In vivo axotomy

Postganglionic nerve crush was performed as previously described (Zaccaria et al., 1998). Briefly, male adult mice were anesthetized by an intra-peritoneal injection of chloral hydrate (400 mg/kg body mass), the right SCG was exposed, and both the internal and external carotid nerves were crushed. The wound was sutured and the mice were left to recover from anesthesia. Mice that had been operated (at least 4 mice for each time point) were killed 1, 24 or 60 days (d) after surgery, for the biochemical experiments, and 1, 6, 12 and 24 d after surgery for the immunohistochemical studies.

2.3. Cell cultures

All reagents used for SCG neuron cultures were from Sigma-Aldrich (Milan, Italy), unless otherwise indicated. Cultures were prepared according to established protocols (Di Angelantonio et al., 2010). SCGs were dissected from P0 to P2 mouse pups of either sex, collected in a pre-warmed L15 medium containing antibiotics (100 unit/ml penicillin and 0.1 mg/ml streptomycin) and cleaned of the surrounding tissues. Ganglia were treated, for 30 min at 37 °C, with 2 mg/ml collagenase in sterile phosphate buffered saline (PBS) and, after collagenase removal, incubated, for 30 min at 37 °C, with 0.5% trypsin in Ca^{2+}-free and Mg^{2+}-free Hanks' balanced salt solution (HBSS). SCG were transferred into warm L15 medium containing 10% fetal bovine serum (FBS) and antibiotics; cells were then mechanically dissociated using a sterile pipette, and their density was determined in a counting chamber. Depending on the type of experiments we performed, cells were plated on either 12 mm coverslips, 25 mm coverslips or 35 mm Petri dishes, at different densities (as indicated in the specific paragraphs), and maintained, at 37 °C and humidified atmosphere with 5% CO_2, in DMEM/F12 medium containing antibiotics, 10% FBS and different NGF concentrations (1, 10, 50 or 100 ng/ml) (Peprotech EC Ltd., London, UK). Both coverslips and plates had been previously coated with 10 μg/ml poly-L-ornithine (3–4 h at 37 °C) and 20 μg/ml laminin (overnight at 37 °C).

2.4. Western immunoblot

The primary antibodies used for Western immunoblots are listed in Table 1.

2.4.1. Preparation of tissue extracts and cell lysates

Six to seven-week old operated wild type and *mdx* mice and matching non-operated controls were anesthetized with isoflurane (Merial, Milan, Italy) and killed by decapitation. Irises and submandibular glands (SbGl) were quickly removed on ice, individually frozen and stored at −80 °C until use. To obtain tissue extracts, each iris was placed in 15 μl of ice-cold RIPA buffer (50 mM Tris/HCl pH 7.6, 150 mM NaCl, 1 mM EDTA, 1% SDS, 1% Triton X-100, 1× inhibitor cocktail, 1 mM PMSF, 0.2 mM Na_3VO_4 and 1 mM NaF) and sonicated for 30 s at a frequency of 30 kHz with a UP100H Ultrasonic Processor (Dr. Hielsher GmbH, Teltow, Germany). In contrast, each SbGl was placed in RIPA buffer (20 μl RIPA/mg fresh tissue mass), triturated with an Ultraturrax and then sonicated.

Cell lysates were obtained from SCG cultures (300,000–500,000/35 mm Petri dishes) by adding 50 μl of the same RIPA buffer used for tissue homogenization directly into the dish, and were collected after 10 min incubation at room temperature (RT). Tissue homogenates and cell lysates were centrifuged (14,000 rpm for 10 min at 4 °C) and a measured aliquot of the supernatant was used to determine protein concentration by using the Micro BCA kit (Pierce, Rockford, IL, USA). Loading buffer (4×: 200 mM Tris/HCl pH 6.8, 4% SDS, 30% glycerol, 4% β-mercaptoethanol, 4% blue bromophenol) was added to the remaining

Table 1
Primary antibodies used in Western immunoblot and immunofluorescence experiments.

Antibody	Dilution	Company
Western immunoblot		
Rabbit anti-tyrosine hydroxylase	1:1000	Millipore (Billerica, MA, USA)
Rabbit anti-actin	1:2000	Sigma-Aldrich (Milan, Italy)
Mouse anti-dystrophin rod domain (Dys1)	1:15	Novocastra Laboratories (Newcastle upon Tyne, United Kingdom)
Mouse anti-dystrophin C-terminal domain (Dys2)	1:10	Novocastra Laboratories
Rabbit anti-TrkA,	3 μg/ml	Abcam (Cambridge, UK)
Mouse anti-phospho-TrkA	1:500	Santa Cruz Biotechnology (Dallas, TX, USA)
Rabbit anti-phospho-TrkA	1:500	Sigma-Aldrich
Rabbit anti-Akt	1:1000	Cell Signaling (Beverly, MA, USA)
Rabbit anti-phospho-Akt	1:1000	Cell Signaling
Rabbit anti-PI3K p85/p55	1:1000	Cell Signaling
Rabbit anti-phospho-PI3K p85/p55	1:1000	Cell Signaling
Rabbit anti-p44/p42 MAPK (ERK1/2)	1:1000	Cell Signaling
Rabbit antiphospho-p44/p42 MAPK (ERK1/2)	1:1000	Cell Signaling
Rabbit anti-S6	1:1000	Cell Signaling
Rabbit anti-phospho S6	1:1000	Cell Signaling
Rabbit anti-eEF1A1 + 2 + L3	1 μg/ml	Abcam
Immunofluorescence		
Mouse anti-neuron specific βIII-tubulin (Tuj1)	1:3000	Covance (Emeryville, CA, USA)
Rabbit anti-caspase 3 cleaved	1:300	Cell Signaling
Mouse anti-β-dystroglycan	1:10	Monosan (Uden, The Netherlands)
Mouse anti-β-dystrobrevin diluted 1:500;	1:500	Transduction Laboratories (Franklin Lakes, NJ, USA)
Rabbit anti-TrkA	1:750	AbCam

supernatant, heated for 5 min at 95 °C and kept at −20 °C until use (Lombardi et al., 2008).

2.4.2. Electrophoresis and immunoblotting

25–40 μg (SCG cell lysate), 10 μg (iris) and 30 μg (SbGl) of protein were loaded on either 4% (Dp427), 7% (dystrophin isoforms), 7.5% (TrkA, ERK1/2) or 10% (all other proteins) sodium dodecyl sulphate-polyacrylamide gel and separated by electrophoresis (SDS-PAGE). HyperPage Pre-stained Protein Marker (Bioline Ltd., London, UK), containing precisely sized recombinant proteins of 190, 125, 80, 50, 40, 25, 20, 15, 10 kDa, was used as the molecular mass standard. After electrophoresis, proteins were transferred onto a nitrocellulose membrane. Non-specific binding sites were blocked with 5% dry milk in 1× TTBS (20 mM Tris/HCl at pH 7.5, 500 mM NaCl, 0.05% Tween 20) and then the membranes were incubated overnight at 4 °C with the primary antibody, diluted in 3–5% bovine serum albumin (BSA) and 0.05% NaN_3 in 1× TTBS. After a thorough rinse in buffer, the membranes were incubated, for 1 h at RT, with either an anti-rabbit IgG or anti-mouse IgG secondary antibody, conjugated with horseradish peroxidase (Promega Italia, Milan, Italy), and diluted 1:5000 in 2.5% dry milk in 1× TTBS. Antibody binding sites were revealed by enhanced chemiluminescence (ECL) (Pierce). The intensity of the bands was evaluated by densitometric analysis using the ImageQuant 5.2 program (Amersham Biosciences Europe, Cologno Monzese, Italy). The optical density (OD) of each protein band was normalized against the OD of the actin or eEFA1 band, used as internal standards. Results from 4 to 14 independent Western immunoblots were averaged and the standard error of the mean (SEM) calculated.

2.5. In vitro axotomy

To perform SCG neuron axotomy *in vitro*, cultures from P0 to P2 wt and *mdx* mouse SCG, prepared as described above, were set up in microfluidic chambers, made of Poly(dimethylsiloxane) (Xona Microfluidics Llc, Temecula, California USA) and formed by two side compartments connected by 450 μm-long micro channels (Taylor et al., 2005; Park et al., 2006). The two compartments were maintained "fluidically" separated by filling them with different volumes of media. The chambers were prepared according to manufacturer's instructions: 35 mm Petri dishes were coated overnight with 10 μg/ml poly-ornithine at 37 °C and then washed and air-dried in a sterile hood. Microfluidic chambers were placed side down on the Petri dishes, sealed by gentle pressure and filled with 20 μg/ml laminin for at least 2 h at 37 °C. The laminin was removed just before plating the cells. Approximately 100,000 cells were pipetted directly into the left-side compartment (soma compartment) of the microfluidic chambers. All compartments were filled with a medium containing 10 or 50 ng/ml NGF, depending on the experiment, and the cells were maintained at 37 °C and 5% CO_2. After 5 d *in vitro*, the entire lane of micro-channels and the adjacent area of the axonal compartment were photographed in phase contrast at a final magnification of 80×, single pictures were pasted in a photomontage (Supplementary Fig. 1), and the axons that emerged in the compartment were counted. Immediately after, the medium in the axonal compartment was substituted with 0.5% trypsin for 30 min at 37 °C, after which the compartment was flushed 3–4 times with fresh medium in order to cut all detached axons and remove the trypsin. Because of fluidic isolation, the soma compartment was affected neither by trypsin incubation nor by axotomy. After this procedure, the axon compartment was filled with fresh medium, and the cells were returned to the incubator. After 22–24 h, the cells were fixed for 30 min at RT and processed for βIII-tubulin immunofluorescence as described in the next section (Immunofluorescence). The entire lane of micro-channels and the adjacent area of the axonal compartment were photographed at a final magnification of 20×, single pictures were pasted in a photomontage, optically zoomed up to 100×, and regenerated axons were counted as above.

In these cultures we performed measurements of the regenerating growth cone area, as axon terminals, recognizable after βIII-tubulin immunolabeling, were confined in their compartment and rarely overlapped to one another. Specifically, acquired pictures were open with the Image J software, optically zoomed up and light enhanced in order to have a better view of the growth cone boundaries. These were, then, manually traced by the operator and measured with the "measure area" macro.

2.6. Immunofluorescence and immunohistochemistry

The primary antibodies used for immunofluorescence and immunohistochemistry studies are listed in Table 1.

2.6.1. Immunofluorescence in cell cultures

The culture medium was removed from the wells with a brief wash in PBS and the cells (20,000–25,000 cells/12-mm glass coverslip) were fixed in 4% paraformaldehyde in PBS with addition of 4% sucrose, for 10 min at RT. After fixation, cells were rinsed and blocked in 1% BSA, 10% normal goat serum (NGS, Jackson ImmunoResearch Europe Ltd., Suffolk, England) and 0.5% Triton X-100 in PBS for 1 h at RT. Primary antibodies were diluted in 1% BSA, 1% NGS and 0.2% Triton X-100 in PBS and incubated overnight at 4 °C. Goat anti-mouse IgG Alexa Fluor 488 and goat anti-rabbit IgG Alexa Fluor 488, diluted 1:1000 (Molecular Probes, Invitrogen), goat anti-mouse IgG Cy3 and goat anti-rabbit IgG Cy3, diluted 1:1000 (Jackson ImmunoResearch), and goat anti-mouse IgG Alexa Fluor 594 diluted 1:1000 (Molecular Probes) were properly used to reveal antigen-antibody binding sites. Cells were incubated with the secondary antibody for 1 h at RT, rinsed in PBS, mounted on glass slides with the ProLong Gold Antifade Reagent (Invitrogen) and observed in a Leica DMIRE2 confocal microscope (Leica Microsystems, Wetzlar, Germany) with a 63× immersion-oil objective. To avoid cross talk between the fluorophores, we carefully adjusted the spectral ranges of the detectors and scanned the images sequentially. Alternatively, a Zeiss Axioskope 2 with either a 63× or 100× immersion-oil objective was used; digital images were acquired and stored by using the AxioVision microscopy software.

2.6.2. Immunohistochemistry on tissue sections

Immunolabeling for tyrosine hydroxylase (TH) was performed on SbGl from control mice and mice subjected to post-ganglionic nerve crush (1, 6, 12 and 24 d). At least 3 mice for each condition were used. Mice were deeply anesthetized by intraperitoneal injection of 0.5 ml/kg body mass of Rompun (20 mg/ml xylazine) (Bayer, Leverkusen, Germany) and 0.5 ml/kg body mass of Zoletil (100 mg/ml tiletamine and zolazepam) (Virbac, Carros, France), and perfused transcardially with an oxygenated Ringer solution, pH 7.3, followed by a fixative composed of 4% freshly depolymerized paraformaldehyde in 0.1 M PB, pH 7.4. Both SbGls, ipsilateral and contralateral to the injury side, were dissected 1 h after perfusion. After overnight cryoprotection in 30% sucrose, SCGs were embedded in OCT compound, cut into 10-μm-thick sections on a cryostat and collected on glass slides. Sections were processed for TH immunohistochemistry using the peroxidase-anti-peroxidase procedure as previously described (De Stefano et al., 1997, 2005). Antibody binding sites were revealed by 3,3′-diaminobenzidine-H_2O_2 reaction developed for 20 min. Negative controls were obtained by omitting the primary antibody. Sections were viewed with a 20× objective at the Zeiss Axioskope 2 light microscope, and digital images were acquired. Selected pictures were processed with Adobe Photoshop to optimize contrast and brightness.

2.7. Standard electron microscopy

Three control (non-operated) and 3 operated mice for each post-operative days (1 d and 24 d) were deeply anesthetized and perfused as described above, by using a fixative composed of 2.5% glutaraldehyde

in 0.1 M PB, pH 7.4. Both ipsilateral and contralateral SCG with their post-ganglionic nerves, irises and SubGl were dissected out and processed for standard electron microscopy. Briefly, tissues were post-fixed for 1 h at 4 °C in 1% osmium tetroxide (OsO_4), rinsed for 1 h in chilled bi-distilled H_2O, and dehydrated in series of ascending ethyl alcohols and propylene oxide, passing through a 20 min *en block* staining with 1% uranyl acetate in 70% ethanol. After an overnight in a mixture of propylene oxide and Epon resin (1:1), specimens were impregnated in pure Epon for 4 h and then polymerized at 60 °C for 3 d. Ultrathin sections (60–70 nm) were cut on a Reichert ultramicrotome, counterstained with 4% uranyl acetate and 0.2% lead citrate, and observed at a Philips EM208S transmission electron microscope operated at 80 kV. Images were acquired with a digital camera (Megaview III, Soft Image System), operated by the AnalySIS software, and processed with Adobe Photoshop to optimize contrast and brightness.

2.8. Quantitative and morphometric analyses

2.8.1. Analysis of TrkA-β-DG and TrkA-β-DB coexistence at the axon terminal

SCG neuron cultures (8000–10,000 cells/12 mm glass coverslips) were fixed after 5 h from plating and processed for TrkA, β-DG and β-DB immunofluorescence as described above. At first, single puncta of TrkA, β-DG and β-DB were quantified by using the ImageJ software on confocal microscope images of 30–35 growth cones/genotype (4 independent experiments). On each picture, the growth cone-like area was first manually traced and measured with the specific ImageJ "Measure Area" function. Successively, images in the red and green channels were separated, adjusted for threshold and binarized. The number of immunopositive puncta was normalized on the respective growth cone-like area (μm^2).

TrkA/β-DG and TrkA/β-DB coexistence in the same subcellular domain was, instead, evaluated by the Coloc function of the Imaris 7.4 software (Bitplane A.G.), applied on the same growth cone images previously used. We first hand-drew a "region of interest" (ROI) over the images, to exclude unlabeled extracellular field and background, and set an unbiased threshold by using the "Automatic Thresholding" function. Because of differences in intensity of labeling and distribution of TrkA, β-DG and β-DB, the degree of their coexistence was evaluated by the Pearson's correlation coefficient, which takes into account the linear correlation between probe labeling intensities, and the Manders' colocalization coefficient, which analyzes the reciprocal colocalization (TrkA/β-DG, TrkA/β-DB and *vice versa*) (for review see Dunn et al., 2011).

2.8.2. SCG neuron morphometric parameters

To evaluate specific morphometric parameters, SCG neuron cultures were processed for βIII-tubulin immunofluorescence. For each genotype (wild type and *mdx*) and NGF concentration (1, 10, 50 or 100 ng/ml), at least three independent experiments (two cultures per experiment) were analyzed. 50–60 neurons per coverslip were photographed with a 40× objective, with a Canon digital camera mounted on a Zeiss Axiophot fluorescence microscope (for a total of 150–180 neurons/experimental point), and analyzed with the ImageJ software. From each neuron, we measured the total neurite length, the number of principal neurites (neurites emerging from the soma) and the branching frequency (number of branching points/total neurite length) (Myers and Baas, 2007). A branch was considered as such only when longer than 5 μm.

A quantitative analysis of possible apoptotic neurons was also performed on SCG neuron cultures grown in the presence of 1 ng/ml of NGF, a very limiting condition for neuronal survival. At this aim, neurons were immunolabeled for both βIII-tubulin and cleaved caspase 3, a marker of apoptosis; nuclei were stained with Hoechst (1:20,000).

Finally, in the attempt to gain more information on the growth cone structure in these types of culture, we labeled SCG neurons, grown either with 10 or 50 ng/ml of NGF, for βIII-tubulin immunofluorescence and Alexa Fluor 488 phalloidin (which labels actin filaments). Phalloidin (diluted 1:100) was added to the fixative, which in this case was composed by 3.7% paraformaldehyde, 0.25% glutaraldehyde, 5 mM EGTA, 1 mM $MgCl_2$, 3% sucrose, 1% Triton X-100 in PBS. After 30 min fixation at RT, we proceeded with βIII-tubulin immunofluorescence as described above.

2.9. Live imaging

Two to four hours after plating, neurons (15,000–20,000 cells plated on 25 mm glass coverslips) were used for live imaging experiments, according to the protocol described by Myers and Baas (Myers and Baas, 2007). The glass coverslips were transferred to a Nikon microscope equipped with an incubator and a heated stage apparatus. Neurons were maintained in 10% FBS, 10 ng/ml NGF in DMEM medium containing 100 unit/ml penicillin and 0.1 mg/ml streptomycin at 37 °C in a humidified atmosphere containing 5% CO_2 for the entire duration of the experiment. Time-lapse images on multiple stage positions were acquired in bright field with a digital camera using a 40× objective. Images were acquired every 10 min (exposure time: 75 ms) for approximately 15 h. The parameters analyzed were growth velocity (μm/min) and the time neurites spent growing, pausing and retracting. To obtain these measures, the "Region measurement" function of the Metamorph software was used. The distance covered by each growth cone was measured frame by frame: moving forward was considered as "growth", moving backward as "retraction" and a displacement of 20 pixels or less (corresponding to 3.22 μm) was counted as a "pause".

2.10. Statistical analysis

Data were expressed as the mean ± SEM and analyzed by using the two-tail Student's *t*-test (which compares two groups at a time), or the chi-squared test. Differences were considered statistically significant for $p \leq 0.05$.

3. Results

3.1. SCG neuron axons of mdx mice projecting to the iris do not recover after post-ganglionic nerve crush

Based on our previous results (De Stefano et al., 2005; Lombardi et al., 2008), a question arose whether, in *mdx* mice, altered noradrenergic innervation by SCG to its peripheral targets, namely iris, heart and SbGl, could depend on intrinsic damages of ganglionic neurons affecting axon growth and differentiation. First, we reactivated the mechanisms of axonal growth by crushing SCG post-ganglionic nerves in adult (5–7 weeks old) wild type and *mdx* mice. Adrenergic re-innervation of iris and SbGl was monitored by evaluating changes in the levels of TH, the rate-limiting enzyme for catecholamine synthesis, within these targets after 1, 24 and 60 d. Representative TH Western immunoblots from wild type and *mdx* mouse iris (Fig. 1A) and SbGl (Fig. 1B) are shown: a band at the expected molecular mass of 62 kDa was detected in all tissue homogenates analyzed. According to our previous observations (De Stefano et al., 2005), in both iris and SbGl, TH levels were significantly lower in *mdx* mice compared to wild type. Therefore, in order to correctly estimate changes in enzymatic levels after post-ganglionic nerve crush, we expressed data as the normalized OD of the immunopositive bands measured after crush *versus* that of the respective control (Fig. 1A' and B'). One day after crush, we observed a significant ($p \leq 0.001$) decrease in TH levels in both wild type (27 ± 11%) and *mdx* (19 ± 10%) mouse irises compared to their respective controls (Fig. 1A'). However, in the following time points, while in the wild type genotype protein levels progressively increased, reaching 55 ± 22% of the control after 60 d, in *mdx* mice they further decreased after 24 d (1.7 ± 1.2%), remaining significantly lower ($p \leq 0.001$) than those in the control even after 60 d (4.1 ± 3%) (Fig. 1A'). A different situation was observed in

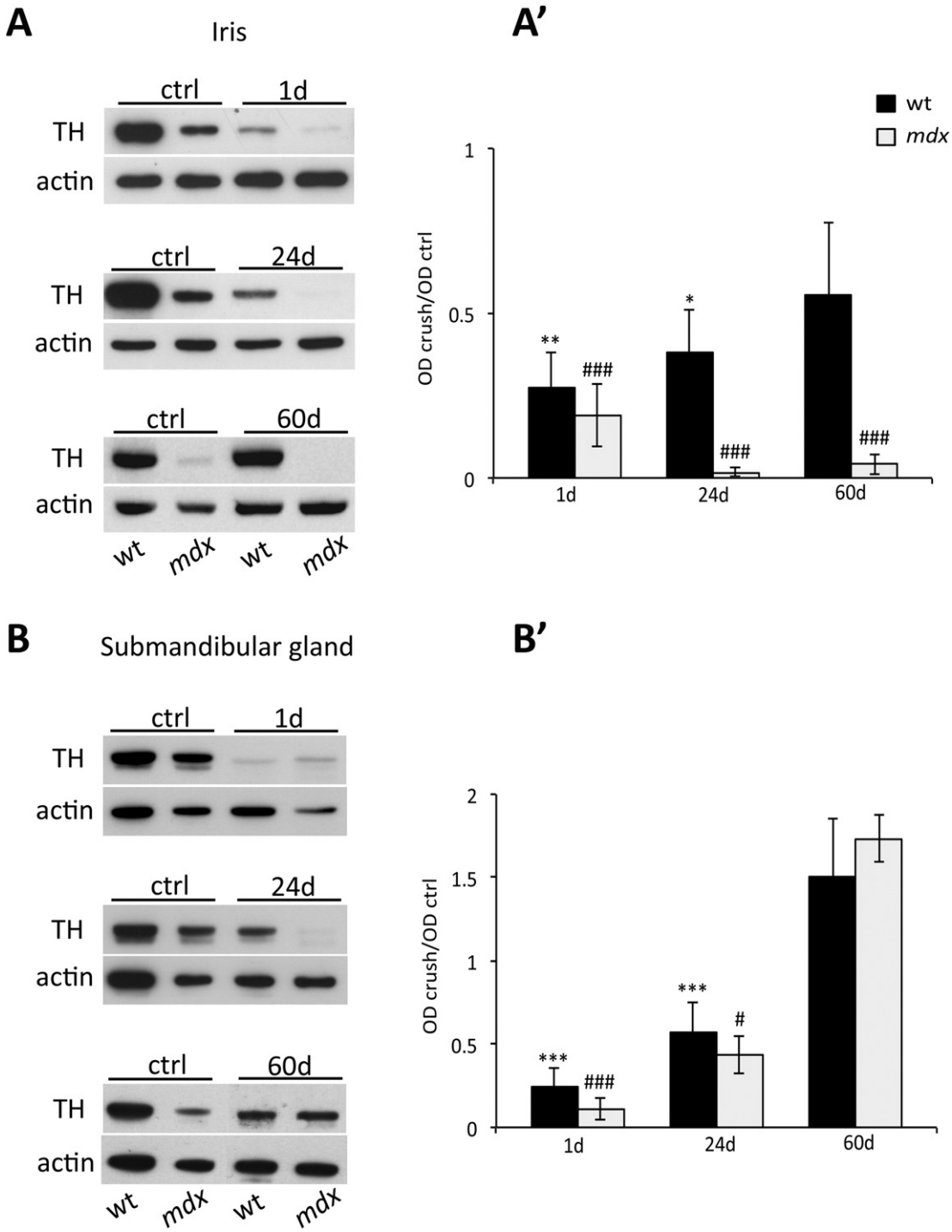

Fig. 1. TH levels do not recover in *mdx* mouse iris after SCG postganglionic nerve crush. Representative Western immunoblots (A–B) and densitometric analysis (A'–B') of tyrosine-hydroxylase (TH) levels in wild type (wt) and *mdx* mouse iris (A) and submandibular gland (B) in control (ctrl) animals and in mice killed 1, 24 and 60 d after post-ganglionic nerve crush. Note that, in both iris and submandibular gland, TH levels in control animals are significantly less in *mdx* mice compared to wt. (A–A') In both wt and *mdx* mouse irises, there is a rapid and drastic decrease in TH level 1 d after crush. However, while in wt mice they begin to recover by 24 d, approaching ctrl levels at 60 d (A', black bars), in *mdx* mice TH levels remain significantly low (A', clear bars). (B–B') In the submandibular gland of both genotypes, TH levels significantly drop below ctrl 1d after crush, and progressively reach and exceed ctrl level by 60 d, with a somewhat slower rate in *mdx* mice (B', clear bars) compared to wt. Data are expressed as the optical density (OD) of the immunopositive bands after crush/OD of the respective ctrl, analyzed by the two-tail Student's *t*-test and represented as the mean ± SEM. $^{*}p < 0.05$, $^{**}p < 0.01$, $^{***}p < 0.001$, is the significance of wt crush *versus* wt control; $^{\#}p < 0.05$, $^{\#\#}p < 0.001$, is the significance of *mdx* crush *versus mdx* control. Actin is used as the internal reference protein. n = 5–8 independent experiments.

the SbGl, where the initial decrease in TH levels (25 ± 11%, wild type; 36 ± 25%, *mdx*) was followed by a progressive increase after both 24 d (71 ± 17%, wild type; 44 ± 14%, *mdx*) and 60 d (150 ± 35%, wild type; 173 ± 26%, *mdx*) (Fig. 1B') from axotomy. However, although final recovery of TH levels in both genotypes was similar, at early time points (*i.e.* at 24 d) it appeared slower in *mdx* mice compared to wild type (Fig. 1B'). Interestingly, in both genotypes, 60 d after axotomy TH levels exceed the respective control levels (1 on the *y* axis), suggesting that both the extent of this target territory and the high amount of NGF here produced could favor an initial hyper-innervation, as

commonly occurs in developmental conditions, which will be pruned later on.

To confirm that the observed decrease in TH protein levels really corresponded to a decrease in noradrenergic innervation, and not just to alterations in TH synthesis and transport by damaged neurons, we performed an immunohistochemical evaluation at the light microscope of the TH immunolabeling in the SbGl of control and operated animals, sacrificed at different dates after post-ganglionic nerve crush (1, 6, 12 and 24 d). For these experiments we chose the sole SbGl, as this target is more densely innervated than iris, which has also the inconvenient of a heavy black pigmentation that irregularly obscures the immunopositive fibers, making evaluation more unreliable. As also previously reported (Lombardi et al., 2008), SbGl of both genotypes is reached by numerous TH immunopositive fibers, which extensively ramify within the tissue (Fig. 2). According to the Western immunoblot results, a drastic decrease in the amount and size of TH-immunopositive fibers was observed at early dates after crush (1, 6 and 12 d), in both wild type and *mdx* mouse SbGl (Fig. 2C, E, wild type; Fig. 2D, F *mdx*), compared to their respective controls (Fig. 2A, wild type; Fig. 2B, *mdx*). TH-immunopositive innervation began to recovery by 24 d (Fig. 2G, wild type; Fig. 2H, *mdx*).

Successively, we verified, by standard electron microscopy, whether post-ganglionic nerve crush induced axonal degeneration within both crushed nerves and their ipsilateral target tissues. These experiments were conducted 1 d and 24 d after axotomy. Ultrathin sections, cut below the site of crush along the post-ganglionic nerves, showed massive axon degeneration in both genotypes (Fig. 3A, wild type; Fig. 3B, *mdx*). No degenerating fibers were observed 24 d after crush; instead, regenerating axons, flanked by reorganizing Schwann cells and embedded in a highly collagenous extracellular matrix, were seen (Fig. 2C, wild type; Fig. 2D, *mdx*). Degenerating fibers were also observed in the iris (Fig. 3E, wild type; Fig. 3F, *mdx*) and SbGl (Fig. 3G, wild type; Fig. 3H, *mdx*) of both genotypes 1 d post-axotomy.

Overall, this first data set suggests that, in *mdx* mice, the integrity of peripheral targets may affect axonal regeneration (the iris smooth muscle is also dystrophic). In addition, ganglionic neurons, intrinsically damaged by the lack of dystrophin, could be less responsive to trophic factors coming from the targets than wild type mouse neurons,

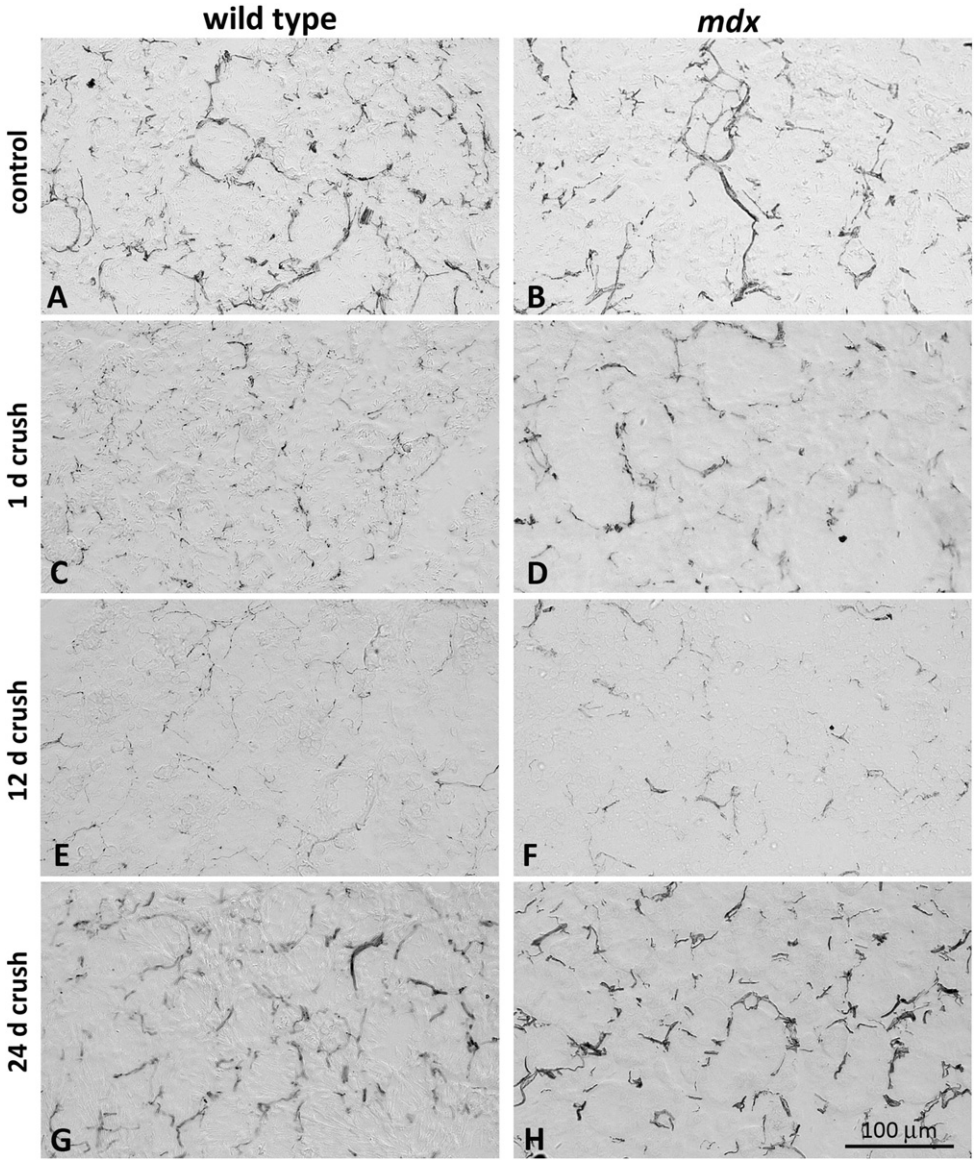

Fig. 2. TH immunopositive fibers decrease in both wild type and *mdx* mouse SbGl after post-ganglionic nerve crush and recover at later stages. Cryosections of SbGl from control (unoperated) wild type (A) and *mdx* mouse (B), show a diffuse net of noradrenergic innervation interspersed within the glandular tissue after TH immunolabeling. Immunopositive fibers drastically decrease 1 d (C, wild type; D, *mdx*) and 12 d (E, wild type; F, *mdx*) after postganglionic nerve crush, and begin to recover after 24 d (G, wild type; H, *mdx*). n = 3 independent experiments for each time point examined after postganglionic nerve crush.

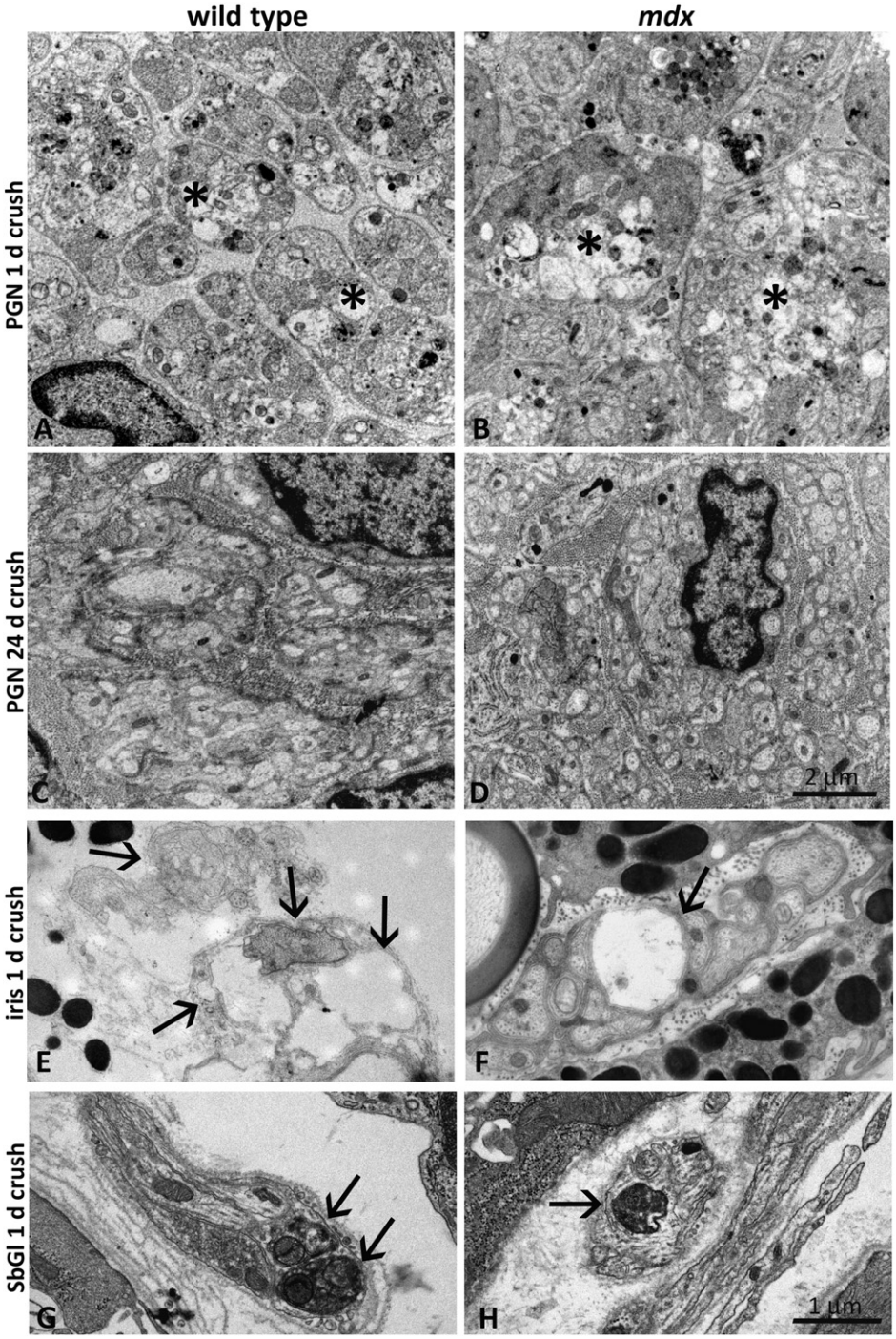

Fig. 3. Electron micrographs showing nerve fiber degeneration after postganglionic nerve crush. (A, B) Ultrathin sections from postganglionic nerves (PGN), cut below the site of damage, show extensive fiber degeneration in both wild type (A) and *mdx* (B) mice, 1 d after axotomy. Some groups of degenerating fibers are indicated by asterisks. (C, D) Twenty-four days after crush, nerve fibers have recovered and images of new regenerating fibers, embedded in collagen-rich extracellular matrix, are seen in both genotypes (C, wild type, D, *mdx*). (E–H) One day after postganglionic nerve crush, degenerating axons (arrows) are seen within the ipsilateral iris (E, wild type; F, *mdx*) and SbGl (G, wild type; H, *mdx*). Scale bar: A–D, 2 µm; G–H, 1 µm. n = 3 independent experiments for each time point examined after postganglionic nerve crush.

especially when these factors are not abundantly expressed. Sympathetic neurons are strictly dependent on NGF for both survival and axon growth (Glebova and Ginty, 2004; Glebova and Ginty, 2005; Reichardt, 2006) and while male mouse SbGl is the major producer of this neurotrophin, much lower amounts are available in the iris (Lombardi et al., 2008). This could be the reason not only for the differences in target innervation observed during pre-natal and post-natal development (De Stefano et al., 2005; Lombardi et al., 2008), but also for those in axon regeneration here reported.

3.2. Cultured mdx mouse SCG neurons exhibit reduced axon regeneration in vitro compared to wild type

To unravel the question whether SCG neurons from dystrophic mice have intrinsic alterations that make them less responsive to NGF, we performed an *in vitro* axotomy by using the microfluidic culture chambers. These are specifically designed to separate, both physically and fluidically, neuron cell bodies from their axons (Taylor et al., 2005): neurons are plated in one compartment (*e.g.* pink side in Fig. 4A) and axons

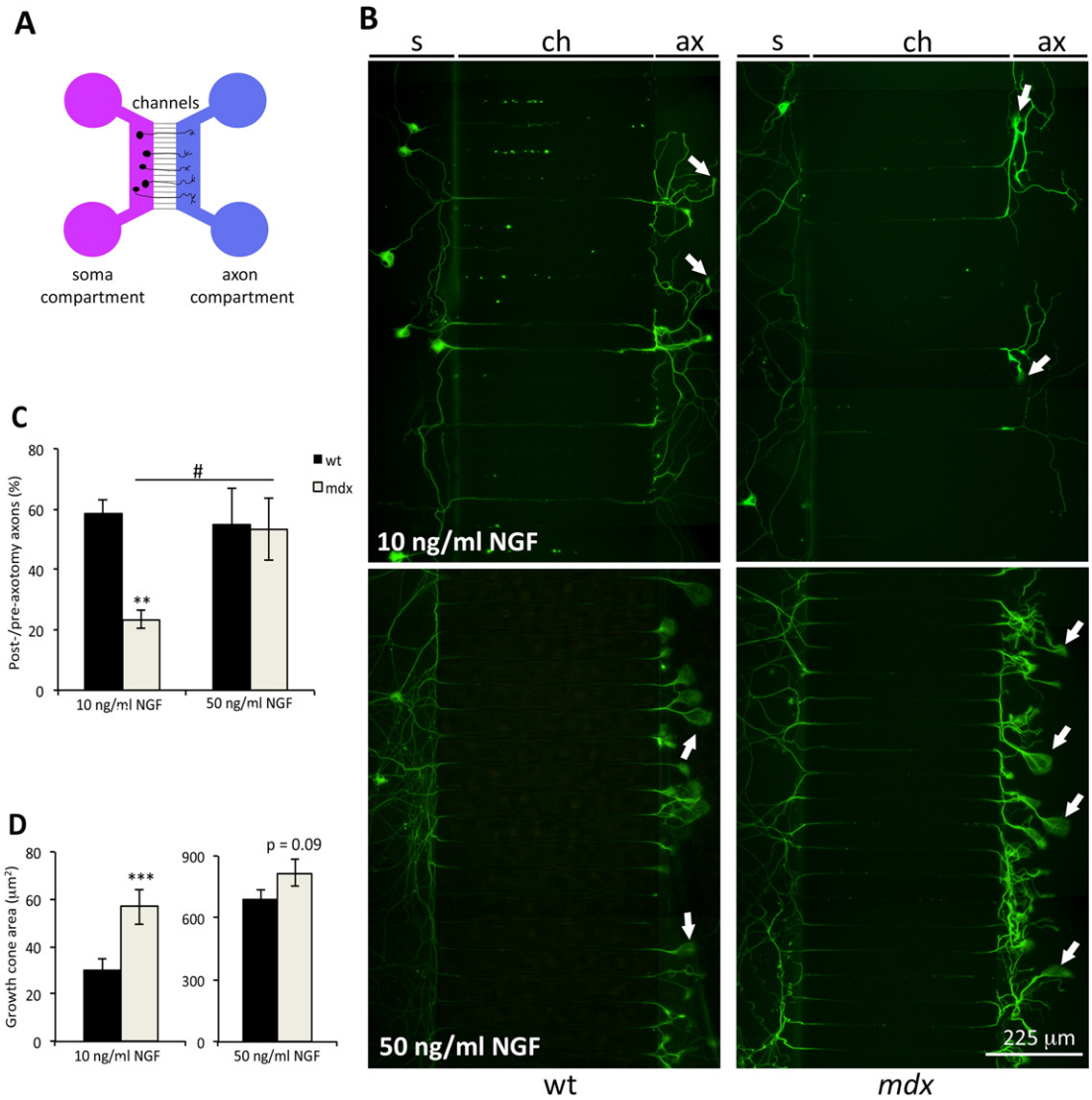

Fig. 4. Cultured *mdx* mouse SCG neurons have reduced regenerative capabilities in the presence of NGF concentration lower than 50 ng/ml. (A) Schematic drawing of a microfluidic chamber. Neurons plated in the "soma compartment" (pink side) extend their axons through micro-channels, reaching the "axon compartment" (blue side). (B) Representative images of wild type (wt) and *mdx* mouse neurons cultured in the presence of either 10 or 50 ng/ml NGF, 22–24 h after axotomy. Neurons are immunolabeled for βIII-tubulin. In the presence of 10 ng/ml NGF, early axon regeneration in *mdx* mouse neuron cultures is dramatically reduced compared to wt. This difference is not observed when neurons are grown in the presence of 50 ng/ml NGF. White arrows indicate some of the growth cones on which morphometric analysis was conducted. s: soma compartment; ch: micro-channels; ax: axon compartment. (C) Quantitative analysis showing the percentage of regenerated axons compared to the pre-axotomy condition. A significant reduction in the regenerative capabilities is observed for *mdx* mouse neurons, with respect to the wt, in the presence of 10 ng/ml NGF. This difference is recovered with 50 ng/ml of NGF. (D) Analysis of growth cone areas measured on regenerated axons shows that *mdx* mouse neurons have significantly larger growth cones compared to wt when grown in the presence of 10 ng/ml of NGF. This difference is reduced ($p = 0.09$) in the 50 ng/ml NGF cultures, when growth cone areas of both genotypes enlarge massively. Data are analyzed by the two-tail Student's *t*-test and represented as the mean ± SEM: $^{***}p < 0.001$; $^{**}p < 0.01$ is the significance of wt *versus mdx*; $^{\#}p < 0.05$ is the significance between consecutive NGF concentrations within the same genotype. $n = 3$–5 independent experiments.

grow into micro-channels, reaching a second compartment (*e.g.* blue side in Fig. 4A). The *in vitro* system has the advantage of both studying ganglion neuron behavior disjointed by the negative/positive influences derived from their targets and regulating the amount of trophic factor provided. We cultured dissociated SCG for 5 d in the presence of either 10 or 50 ng/ml of NGF, added to both compartments. Axons growing in the side compartment were first counted in phase contrast (Supplementary Fig. 1), and then a combined chemical (trypsin treatment) and mechanical (medium flushing) axotomy was performed. Axons were allowed to regenerate for 22–24 h and the new emerging axons, immunolabeled for βIII-tubulin (Fig. 4B), were counted. Before axotomy, the number of axons exiting the micro-channels after 5 d *in vitro* was usually higher in wild type mouse SCG cultures compared to *mdx*, especially in the 10 ng/ml NGF condition (Supplementary Fig. 1). However, the number of axons varied also within the same genotypes, depending on the number of neurons, which adhered close enough to the channels. For this reason, we expressed the number of regenerated axons as the percentage with respect to their pre-axotomy condition. According to the *in vivo* results, *mdx* mouse neuron axons regenerated significantly ($p \leq 0.01$) slower than wild type in the presence of 10 ng/ml NGF (regenerated axons: wild type, 58 ± 4%; *mdx*, 23 ± 3%) (Fig. 4C). When cultured and axotomized in the presence of 50 ng/ml NGF, *mdx* mouse neurons increased significantly their regenerative capability, while that of wild type mice remained stable, and differences between the two genotypes were abolished (regenerated axons: wild type, 55 ± 12%; *mdx*, 45 ± 12%) (Fig. 4C). For *mdx* mouse neurons, this last result is compatible with the regenerative performance previously observed in the SbGl *in vivo*. In contrast, for wild type mouse neurons, the fact that axon re-growth does not positively correlate with the amount of trophic factor (see the next section) could be ascribed to the

restrictive experimental conditions compared to the *in vivo* situation. Specifically, in these experiments we counted the number of axons regrowing through a limited number of channels, with the additional variable of the number of neurons close enough to the channels themselves. It is, therefore, conceivable that the response to NGF by wild type mouse neurons was already efficient at the lower NGF concentration and that a better performance in axon regeneration might not be clearly appreciated due to the physical limitations of the experimental device. In contrast, the reduced responsiveness of *mdx* mouse neurons to NGF allows one to appreciate a significant dose-dependent difference in axon regeneration.

A further observation was that the regenerating axons of *mdx* mouse neurons exhibited significantly ($p = 0.009$) larger growth cones compared to wild type when grown in the presence of 10 ng/ml NGF, a difference that was reduced ($p = 0.09$) by the higher NGF concentration (Fig. 4D). Large growth cones emerging from the microfluidic channels are indicated by arrows in Fig. 4B; their bulbous shape is a common feature in regenerating growth cones, as it derives from extensive microtubule accumulation, often accompanied by a retrograde turn of microtubule plus ends (reviewed in Bradke et al., 2012). These structures are very common also in our regenerating axons, especially in *mdx* mouse neuron cultures. According to the literature (Dent et al., 1999; Dent and Kalil, 2001; Ren and Suter, 2016) large growth cones are usually indicative of pausing growth cones, characterized by retrograde looping of the microtubule plus ends, which halts axon growth. On the other hand, SCG neuron growth cone extension and axon growth are linearly dependent on NGF concentration. Therefore, following crush *in vitro*, we may face both situations: enlargement due to halted growth in *mdx* mouse neurons (mainly at 10 ng/ml) and enlargement due to higher NGF availability in both genotypes (50 ng/ml). Considering the intense βIII-tubulin immunolabeling decorating these bulbous growth cones, the idea is of structures mostly enriched in microtubules and little in actin. Unfortunately we could not perform a high-resolution study within the microfluidic chamber, as these must adhere on a plastic well, which blurs the image at high magnifications. Therefore, to gain some more information, we used SCG neuron cultures grown for 24 h in the presence of either 10 or 50 ng/ml NGF and performed immunofluorescence for βIII-tubulin in combination with either anti-actin antibodies or Alexa Fluor 488-conjugated phalloidin. In any of the cases, actin detection was extremely difficult to achieve, and after several different protocols we finally could get some staining. As shown in Supplementary Fig. 2, phalloidin labeling reveals a very poor actin cytoskeleton, which does not go too far from the usually large core of microtubules, and it is easily concealed by the intense βIII-tubulin immunolabeling. Nevertheless, we could notice that indeed growth cones of *mdx* mouse neurons tended to be larger than those of the wild type, at both NGF concentrations. Although their shape is definitively different from that observed after crush *in vitro*, as also noticeable by the live imaging pictures and videos (in this paper), several growth cones of *mdx* mouse neurons contain looping microtubules at both NGF concentrations (Supplementary Fig. 2).

Taken together, these data suggest altered cytoskeletal dynamics at the growth cone of *mdx* mouse neuron regenerating axons, which could be more pronounced in the presence of low amounts of trophic support.

3.3. Cultured SCG neurons from mdx mice are less responsive to NGF compared to wild type

To further verify whether *mdx* mouse neuron sensitivity to NGF was reduced also in early growth conditions, we set up "target-free" SCG cell cultures from P0 to P2 wild type and *mdx* mice in the presence of different NGF concentrations: 1 ng/ml (barely enough to support sympathetic neuron survival and differentiation *in vitro*), 10 ng/ml (intermediate concentration), 50 ng/ml (normally used, according to the literature) (Wyatt and Davies, 1995; Kohn et al., 1999; Tsui-Pierchala and Ginty, 1999) and 100 ng/ml (very high concentration). Neurons were grown for 5 h, a time sufficient to extend neurites long enough to be measured, and then immunolabeled for the neuron-specific βIII-tubulin. Before performing morphometric analyses we ensured, by Western immunoblot on random cultures, that wild type mouse neurons expressed Dp427 once placed *in vitro*, at the same time verifying its absence in *mdx* mouse neuron cultures (Fig. 5A). As expected, the Dys1 antibody always revealed a single clear band of 427 kDa in the cell lysates from wild type mice, but never in those from *mdx* mice. Moreover, we also verified whether shorter Dys isoforms were expressed *in vitro*, as previously demonstrated *in vivo* (De Stefano et al., 1997), and whether their expression varied between the two genotypes. The Dys2 antibody, which recognizes all dystrophin isoforms, labeled an intense band at 260 KDa and three much less intense bands at approximately 140, 116 and 71 KDa (Fig. 5A). All isoforms were expressed by both genotypes, and were the same previously identified *in vivo*, with the difference that *in vivo* the most prominent isoform was the 116 kDa expressed by Schwann cells. In Fig. 5B, a representative image of wild type and *mdx* mouse neurons, immunopositive for βIII-tubulin and grown in the presence of 1 and 50 ng/ml of NGF, is shown. Almost all neurons of both genotypes extended one or more principal neurites when cultured with medium-high NGF concentrations (10, 50 or 100 ng/ml). However, when only 1 ng/ml NGF was added to the culture medium, a significantly higher percentage (51 ± 2%) of *mdx* mouse neurons, compared to wild type (30 ± 4%), did not elongate neurites (Fig. 5C). When 10 ng/ml NGF was added, the percentage of wild type mouse neurons did not change significantly (26 ± 4%) compared to the 1 ng/ml NGF condition, whereas that *mdx* mouse neurons decreased significantly (29 ± 4%), abolishing the differences between the two genotypes (Fig. 5C). Since 1 ng/ml NGF is limiting for neuron survival, we also verified the number of apoptotic neurons by co-immunolabeling βIII-tubulin and activated caspase 3, a classical marker of apoptosis. The number of dying neurons was significantly ($p < 0.05$) higher in *mdx* mouse neuron cultures compared to wild type: 6.81% of *mdx* mouse neurons were caspase 3 immunopositive *vs* 3.43% of wild type mouse neurons. Representative images of apoptotic *mdx* mouse neurons are shown in Supplementary Fig. 3. Therefore, these data indicate that extreme NGF concentrations affect both neuron survival and ability to elongate new neurites in *mdx* mouse cultures compared to wild type.

Successively, we performed a morphometric/quantitative analysis at all different NGF concentrations, evaluating parameters such as: the number of principal neurites emitted by each neuron, the total neurite length and the branching frequency (Myers and Baas, 2007; Kim et al., 2006). For both wild type and *mdx* mouse neurons, the number of principal neurites emerging from neuronal cell bodies increased in parallel with the increase in NGF concentration in the medium (Fig. 5D), confirming once more the strict dependence of sympathetic neurons on this trophic factor. However, values for *mdx* mouse neurons were always significantly lower ($^{*}p \leq 0.05$ and $^{***}p \leq 0.001$) compared to wild type. A similar pattern was observed for the total neurite length (Fig. 5E). In contrast to these parameters, the branching frequency (Fig. 5F), expressed as the number of branching points/total neurite length (Myers and Baas, 2007), was neither different between the two genotypes nor changed in the interval between 10 and 100 ng/ml NGF. The only exception in this trend was when SCG neurons were cultured in the presence of 1 ng/ml NGF, a concentration at which *mdx* mouse neurons showed a significantly lower ($p \leq 0.001$) branching frequency compared to wild type.

Taken together, these data show a decrease in NGF sensitivity by *mdx* mouse neurons compared to wild type for a wide range of NGF concentrations, which specifically affects neurite emission, early neurite growth and, to a much lesser extent, neurite branching.

3.4. Early neurite growth dynamics of mdx mouse SCG neurons is altered compared to wild type

To investigate the possibility that the observed alterations in *mdx* mouse neurite growth relied on altered growth dynamics, we performed

a live imaging study by time-lapse photography. SCG neurons were cultured in the presence of 10 ng/ml of NGF, a concentration of neurotrophin sufficient for survival, but still able to highlight significant differences in neurite growth between the two genotypes. Two to four hours after plating, neurons were transferred under a light microscope, equipped with a cell culture incubator and a heated stage, and a series of pictures was

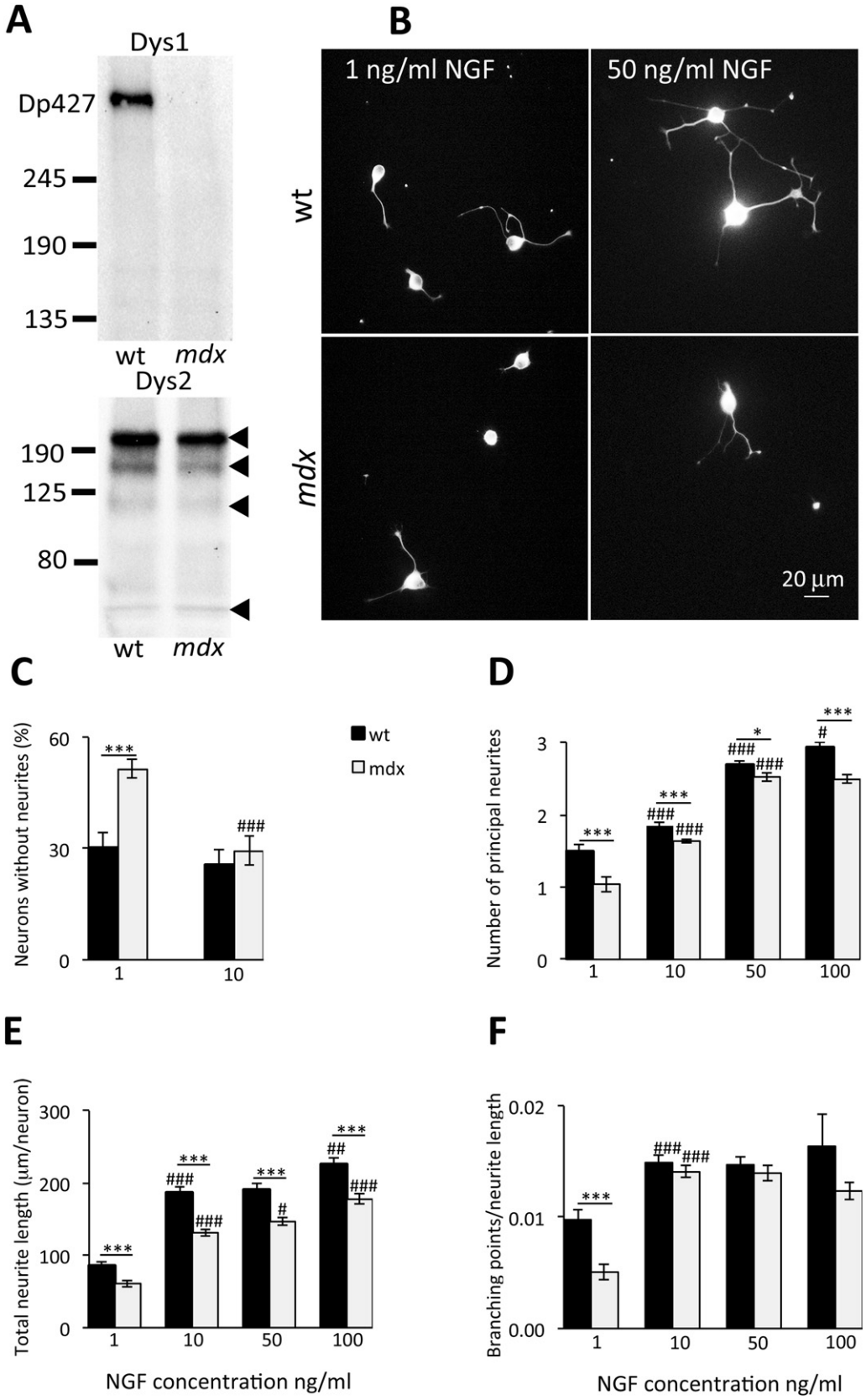

acquired over 15 h. The time neurites spent advancing, pausing and retracting, as well as the velocity of growth and retraction (μm/min), were measured in individual photograms and compared for statistical analysis. An illustrative time-lapse sequence of collected images (0, 160 and 320 min of recording) is shown in Fig. 6A. After 3–5 h, most of the neurites had already grown out of the photographic field (or were completely retracted). In wild type mouse neuron cultures, neurites emerging from somata immediately branched several times, with neurons becoming highly ramified in a short time (Fig. 6A left column; representative live imaging video at http://bbcd.bio.uniroma1.it/video/video1wtscg.mp4). In contrast, in *mdx* mouse neuron cultures, neurite growth dynamics was altered compared to wild type, at least during the first few hours, as they stopped and retracted quite frequently, therefore taking more time to advance (Fig. 6 right column; representative live imaging video at http://bbcd.bio.uniroma1.it/video/video2mdxscg.mp4). Analysis of the different parameters taken into consideration showed that neurites of *mdx* mouse neurons spent significantly less time in advancing (21%; $p < 0.001$) and more time in pausing (16%; $p < 0.001$) and retracting (5.5%; $p < 0.01$), compared to wild type (Fig. 6B). The growth and retraction velocities of moving growth cones, however, were not different between the two genotypes (not shown).

Taken together, these data suggest that, in *mdx* mouse SCG neurons, growth cone advancement and neurite growth is altered with respect to the wild type.

3.5. TrkA-NGF signaling is reduced in mdx mouse SCG neurons compared to wild type

We verified whether the differences in axon/neurite regeneration and growth between wild type and *mdx* mice could depend on alterations in NGF signaling. Protein levels of TrkA receptor, phosphorylated TrkA (*p*TrkA) and of kinases downstream NGF signaling within the growth cone, both phosphorylated and non-phosphorylated, *i.e.* phosphatidylinositol-3-kinase (PI3K) and *p*PI3K, Akt and *p*Akt, Erk1/2 and *p*Erk1/2, were analyzed in both wild type and *mdx* mouse SCG neurons cultured in the presence of either 10 ng/ml or 50 ng/ml NGF. Representative Western immunoblots are shown in Fig. 7A. Levels of all non-phosphorylated proteins were usually similar between the two genotypes, at both 10 and 50 ng/ml NGF. Except the PI3K and Erk1/2, which were significantly higher (PI3K: $p < 0.05$, with 50 ng/ml NGF; Erk1/2: $p < 0.05$, with 10 ng/ml NGF) in *mdx* mouse neurons compared to wild type. Levels of *p*TrkA and of phosphorylated signaling proteins were all significantly lower in *mdx* mouse neuron cultures compared to wild type in the presence of 10 ng/ml NGF (*p*TrA: $p < 0.001$; *p*Erk1/2, *p*PI3K, *p*Akt: $p < 0.05$) (Fig. 7A'). At higher NGF concentrations, *p*TrkA levels did not vary between the two genotypes, while those of all the other proteins were significantly different: *p*PI3K increased ($p < 0.01$) in *mdx* mouse neurons compared to wild type (in parallel with its non-phosphorylated form), while *p*Erk1/2 and *p*Akt remained lower ($p < 0.05$ – $p < 0.001$)

These data show a reduction in the levels of activation of TrkA receptors in *mdx* mouse sympathetic neurons, compared to wild type, grown in the presence of 10 ng/ml NGF. This reduction leads to a decrease also in the two TrkA-associated signaling cascades active at the growth cone, here analyzed. At higher NGF concentrations, the level of activation of TrkA receptors is apparently similar between the two genotypes, but the downstream signaling persists in being less activated in the dystrophic genotype.

3.6. TrkA receptors co-localize with proteins of the DGC in growth cones of both wild type and mdx mouse neurons

Upon NGF binding, TrkA receptors are recruited and stabilized within lipid rafts (Limpert et al., 2007), which contain caveolins, a class of proteins that also binds to the DCG (Huang et al., 1999; Noël et al., 2009). No data in the literature have ever described co-occurrence, within the same cellular domain, of TrkA with DGC components. However, one of our hypotheses, which could explain the reduced sensitivity of *mdx* mouse neurons to NGF, is that the DGC, deprived of Dp427, may not properly link to lipid rafts. These, in turn, could not efficiently cluster and stabilize TrkA receptors, with consequent reduction in its intracellular signaling. We, therefore, co-immunolabeled cultured wild type and *mdx* mouse SCG neurons for TrkA and either β-DG (Fig. 6A) or β-DB (Fig. 6B), two major components of the DGC, to verify whether these proteins co-occurred at the same cellular domains. Confocal microscopy analysis showed an intense immunolabeling for all three proteins within neuron somata, which represent the site of synthesis, and a discrete, punctuate immunolabeling along neurites and within growth cones (enlarged boxed areas in Fig. 8A and B). Also in this experimental condition, growth cones of *mdx* mouse neurons appeared usually larger than those of the wild type, as observed in the microfluidic chamber experiments. In both wild type and *mdx* mouse neuron growth cones, TrkA receptor (Fig. 8A and B), β-DG (Fig. 8A) and β-DB (Fig. 8B) appeared diffusely distributed, partially coexisting in the same sub-domain, as suggested by the yellow spots of superimposition of the green (TrkA) and red (either β-DG or β-DB) immunofluorescences (enlarged boxed areas in Fig. 8A and B). At first, we quantified the number of immunopositive puncta/μm^2 for each protein, by using the ImageJ software. The results, graphically reported in Fig. 8C, showed no differences, between the two genotypes, in the number of TrkA-immunopositive puncta, but a significant decrease, in *mdx* mouse neurons compared to wild type, in both β-DG and β-DB immunopositive puncta. As colour merge of two channels is not a warranty of protein colocalization and interpretation could result ambiguous for intermediate colors, TrkA/β-DG and TrkA/β-DB coexistence in a same domain was analyzed and quantified by using the Coloc function of the Imaris software, which calculates both Pearson's Correlation Coefficient (PCC) and Manders' Colocalization Coefficient (MCC). Results are reported in Table 2. First and important data is that TrkA receptors co-occurred in the same cellular domains with both β-DG and β-DB, as the PCC were all above 0: colocalization values ranged mainly between low (0–0.3) and moderate (0.3–0.7), 1 corresponding to perfect linear correlation between two fluorescence intensities and −1 to perfect inverse correlation. Differences between wild type and *mdx* mouse neurons were not statistically

Fig. 5. Cultured *mdx* mouse SCG neurons are less sensitive to NGF compared to wild type. (A) Western immunoblots of SCG neuron lysates after 5 h in culture. The Dys1 antibody confirms that wild type (wt) mouse cells express the high molecular mass dystrophin (Dp427). As expected, Dp427 is absent in *mdx* mouse cell cultures. The Dys2 antibody, which recognized all dystrophin isoforms, reveals an intense immunopositive band of 260 kDa, and fainter bands at 140, 116 and 71 kDa (indicated by arrowheads on the right side). All dystrophin isoforms are expressed by both wild type and *mdx* mouse neurons. On the left side of both Western immunoblots, the molecular mass standards (kDa) are indicated. (B) Representative pictures of wt and *mdx* neurons, immunolabeled for βIII-tubulin, after 5 h in culture in the presence of either 1 or 50 ng/ml NGF. Neurites emerging from cell bodies are more numerous and longer in wt mouse neuron cultures compared to *mdx*. (C–F) Quantitative and morphometric analyses on wt and *mdx* mouse SCG neurons cultured in the presence of either 1, 10, 50 or 100 ng/ml NGF. (C) Number of neurons without neurites cultured with 1 or 10 ng/ml NGF. At the lowest NGF concentration, significantly more *mdx* mouse neurons lack neurites compared to wt. This number significantly reduces in the 10 ng/ml NGF condition, becoming comparable to wt. (D) The mean number of principal neurites/neuron increases in an NGF-dependent manner for both genotypes. However, *mdx* mouse neurons always exhibit significantly fewer neurites compared to wt. (E) The total neurite length (expressed as μm/neuron) increases in an NGF-dependent manner for both genotypes. However, *mdx* mouse neurons always exhibit significantly shorter neurites compared to wt. (F) The branching frequency (expressed as the number of branching points/total neurite length per neuron) is not affected by NGF starting from the 10 ng/ml concentration, but it is significantly reduced in the presence of 1 ng/ml NGF, for both genotypes. Moreover, at this concentration, the number of branches is significantly less in *mdx* mouse neurons compared to wt. Data are analyzed by the two-tail Student's *t*-test and represented as the mean ± SEM: $^{*}p < 0.05$, $^{**}p < 0.01$, $^{***}p < 0.001$ is the significance of wt *versus mdx*; $^{\#}p < 0.05$, $^{\#\#}p < 0.01$, $^{\#\#\#}p < 0.001$ is the significance between consecutive NGF concentrations within the same genotype. n of neurons = 301 wt and 319 *mdx* (1 ng/ml NGF); 490 wt and 602 *mdx* (10 ng/ml NGF); 411 wt and 410 *mdx* (50 ng/ml NGF); 314 wt and 312 *mdx* (100 ng/ml NGF).

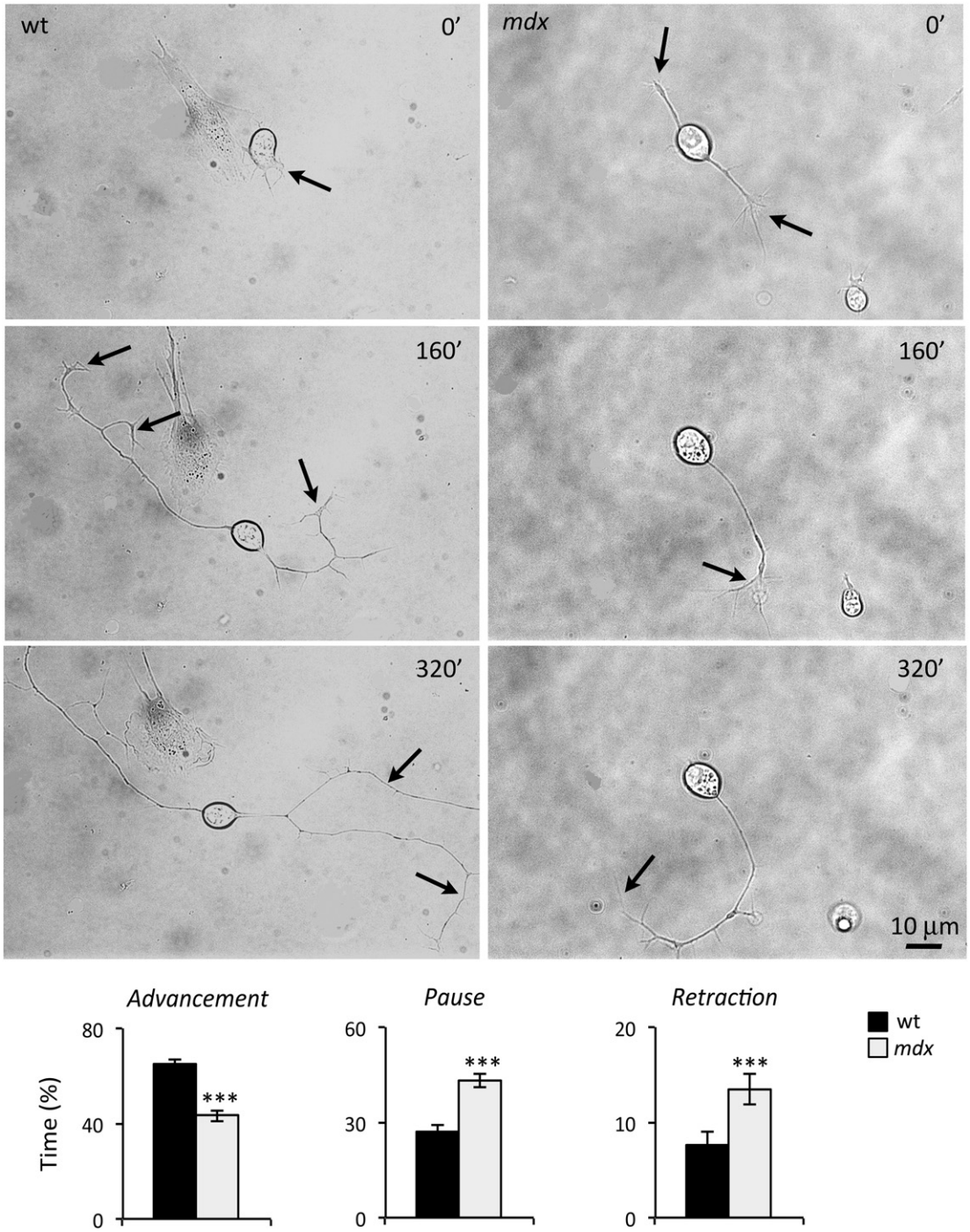

Fig. 6. *mdx* mouse neuron axons spend less time in advancing and more in pausing and retracting compared to wild type. Representative images from time-lapse recordings of wild type (wt) and *mdx* mouse neurons, cultured in the presence of 10 ng/ml NGF, taken at 0 min (0′, just before recording started), 160 min (160′) and 320 min (320′). Arrows indicate neurites and their growth cones; Below images, quantitative analyses of the percentage of time that growth cones of wt and *mdx* mouse neuron axons spend in advancing, pausing and retracting during time-lapse recording. In *mdx* mouse neuron cultures, growth cone advancement is significantly reduced compared to wt, while pausing and retraction are significantly increased. Measurements were done on 39 wt mouse neurons (for a total of 182 growth cones observed) and 47 *mdx* mouse neurons (for a total of 197 growth cones observed). Data are analyzed by the two-tail Student's *t*-test and represented as the mean ± SEM: $^{**}p < 0.01$, $^{***}p < 0.001$.

different by the Student's *t*-test. As probes were differently distributed (spots of TrkA immunolabeling outnumbered those of β-DG and β-DB), application of the MCC provided information on both the fraction of TrkA colocalizing with either β-DG or β-DB, and that of β-DG and β-DB coexisting with TrkA. As intuited, in the growth cones of both genotypes, a larger fraction of β-DG and β-DB coexisted with TrkA than *vice versa*. In this case, the differences between wild type and *mdx* mouse neurons reached statistical significance for the β-DB/TrkA ratio, which was higher in the wild type (Table 2).

A novel and important finding of these experiments is that TrkA receptors in SCG neurons can co-occur within the same sub-cellular domains with the DGC.

4. Discussion

Proper axonal growth dynamics is important for neural circuit establishment and remodeling. These processes are guided by coordinated neuron-target organ signaling, whether they occurred during

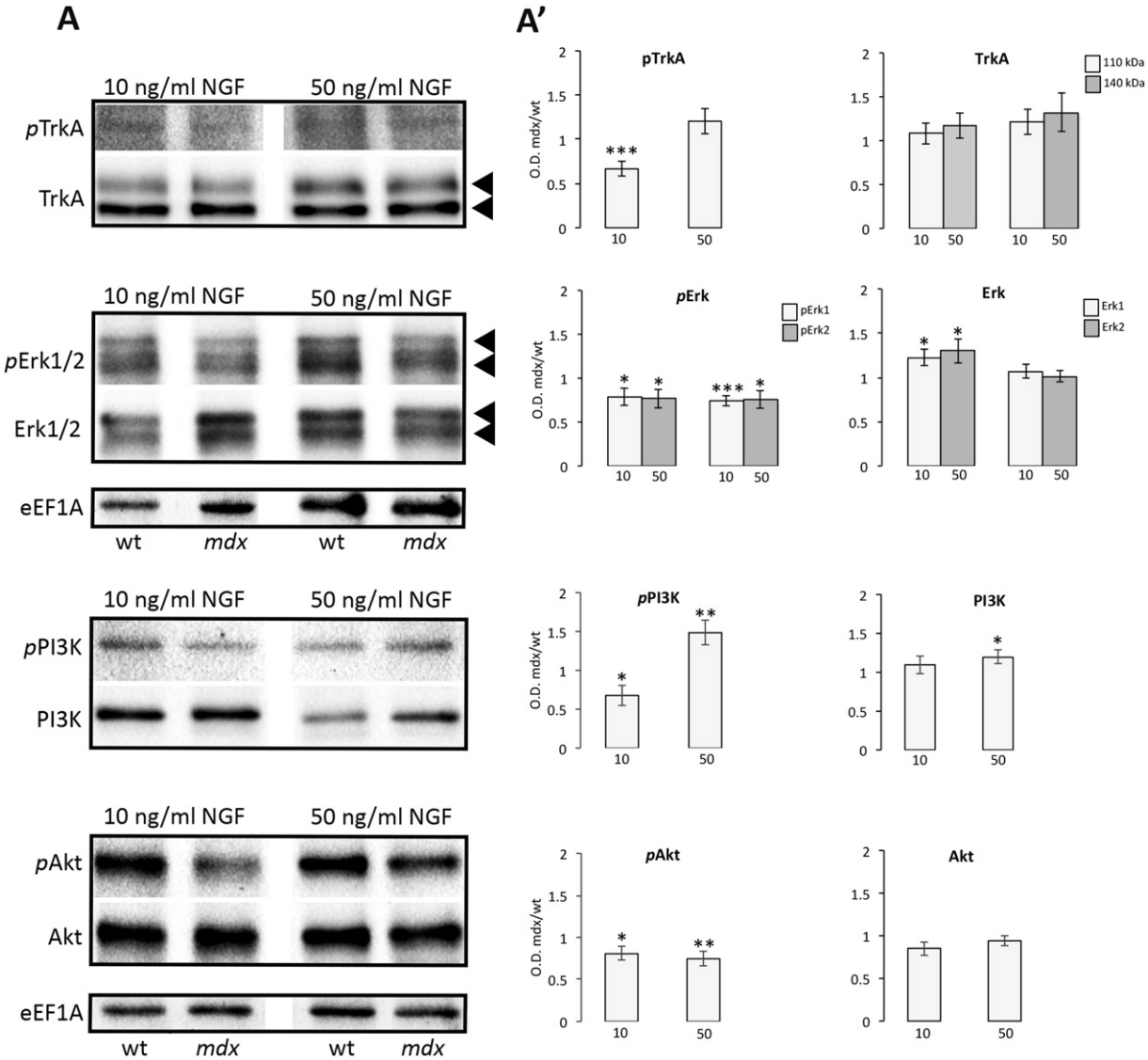

Fig. 7. NGF/TrkA signaling cascade is reduced in cultured *mdx* mouse SCG neurons compared to wild type. Representative Western immunoblots (A) and densitometric analyses (A') of protein levels of TrkA receptor, phosphorylated TrkA (*p*TrkA), and its downstream signaling kinases PI3K, *p*PI3K, Akt, *p*Akt and Erk1/2, *p*Erk1/2. SCG neurons were cultured for 5 h in the presence of either 10 or 50 ng/ml of NGF. In the 10 ng/ml NGF culture condition, protein levels of *p*TrA and of its intracellular signaling molecules are significantly reduced in *mdx* mouse neurons compared to wild type (wt). The corresponding non-phosphorylated proteins do not vary between the two genotypes, except for the Erk1/2, which are both higher in *mdx* mouse neurons compared to wt. In the 50 ng/ml NGF condition, TrkA protein levels, both phosphorylated and non-phosphorylated, are similar between the two genotypes. This reflects in a significant increase in both total and phosphorylated pPI3K in *mdx* mouse neurons compared to wt, but *p*Akt and *p*Erk1/2 persists to be significantly lower. Data are expressed as the ratio between the optical density (OD) of the immunopositive bands in *mdx* mouse cell lysates/OD in wt cell lysates (OD *mdx*/wt), analyzed by the two-tail Student's *t*-test and represented as the mean ± SEM. $^{*}p < 0.01$; $^{**}p < 0.05$; $^{***}p < 0.001$. The elongation factor 1A (eEF1A) was used as the internal reference protein n = 6–14 independent experiments.

development or adulthood. In this study we highlighted a novel role of Dp427, intimately connected to NGF intracellular signaling, in both early axonal growth and regeneration of SCG autonomic neurons.

4.1. Dp427 is important for NGF-dependent early axonal growth and regeneration

We previously reported (De Stefano et al., 2005; Lombardi et al., 2008) that loss of Dp427 in dystrophic *mdx* mice induce an early and persistent reduction in the noradrenergic innervation of iris and heart by the sympathetic SCG, which is associated with a significant loss of muscle-innervating ganglionic neurons. This at first suggested that lack of Dp427, by altering structure and physiology of cardiomyocytes and iris smooth muscle cells, could retrogradely affect proper SCG neuron projection and survival. On the other hand, SbGls (a non-muscular target of SCG) showed a reduction in terminal axon defasciculation and sprouting of noradrenergic innervation, which also suggested the presence of intrinsic neuronal alterations affecting axon plasticity. Among these, alterations in components of the NGF signaling complex highlighted a direct and/or indirect role of Dp427 in this trophic pathway (Lombardi et al., 2008). Results obtained in this study on the regenerative capabilities of sympathetic neurons after post-ganglionic nerve crush *in vivo* and *in vitro* confirm both previous hypotheses. In *mdx* mice, complete failure of iris re-innervation by axotomized neurons, but simultaneous successful recovery of the sympathetic network in the SbGl of the same animals, along with successful reinnervation of both targets observed in wild type mice, indicates that dystrophic muscles indeed retrogradely affect the capability of autonomic neurons to

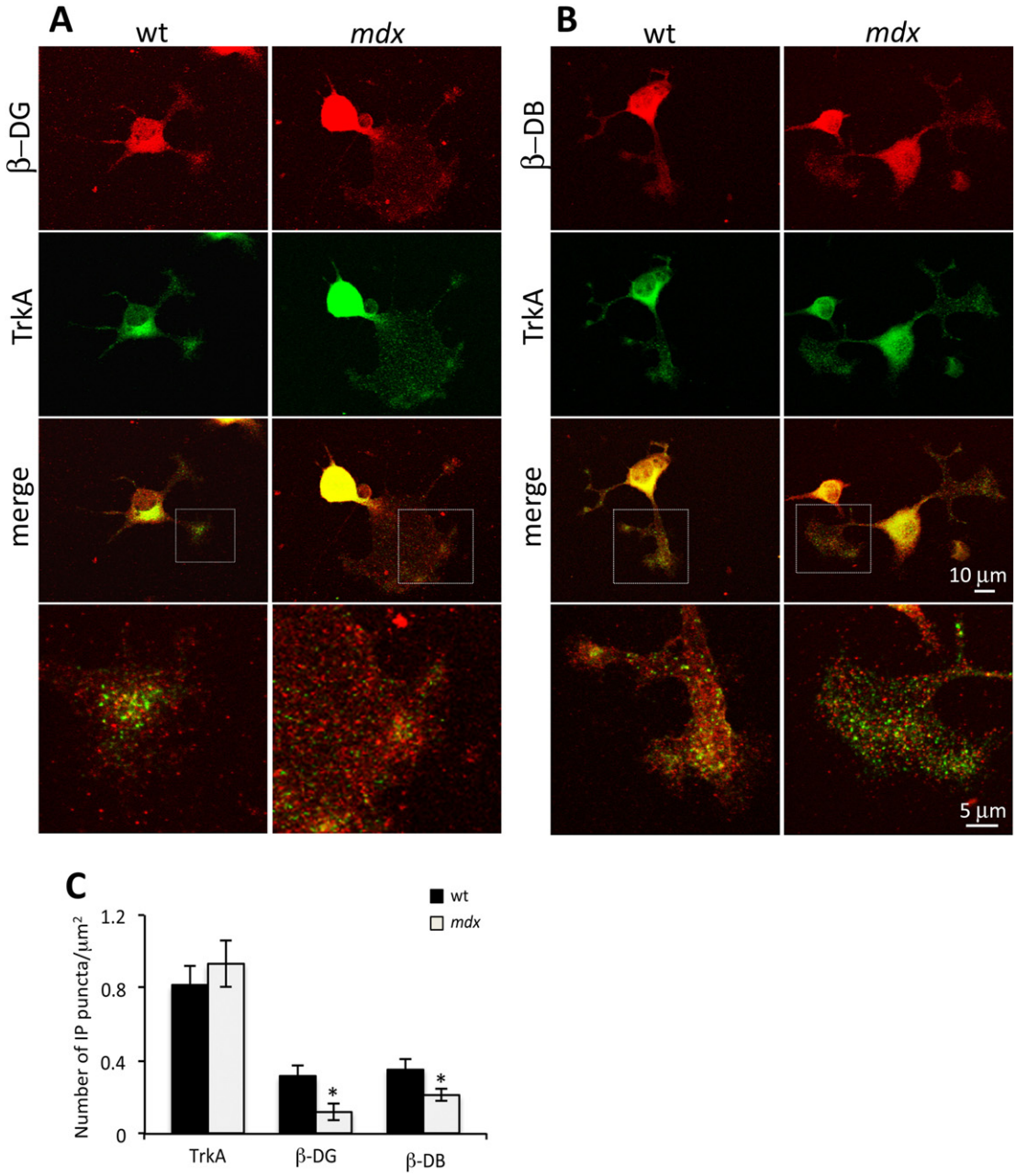

Fig. 8. TrkA, β-dystroglycan and β-dystrobrevin coexistence in the growth cones of SCG neuron axons *in vitro*. Representative pictures of TrkA/β-dystroglycan (β-DG) (A) and TrkA/β-dystrobrevin (β-DB) (B) double immunolabeling in wild type (wt) and *mdx* mouse SCG neurons, cultured for 5 h in the presence of 10 ng/ml NGF. The growth cones in the boxed areas in the "merge" panels are enlarged below the corresponding picture. All proteins appear as a punctiform labeling decorating the growth cone areas. By pure observation, the extent of co-localization of TrkA with both β-DG and β-DB (yellow spots in the merge panels) in the growth cones of *mdx* mouse neurons seems to be reduced compared to wt. Growth cones of *mdx* mouse neurons are characteristically enlarged. (C) Quantitative analysis of the number of immunopositive (IP) puncta, normalized per μm^2 of the growth cone area, counted on 30–35 growth cones/genotype. The number of TrkA immunopositive spots is similar between the two genotypes, while those of β-DG and β-DB are significantly less in *mdx* mouse neurons compared to wt. Data are analyzed by the two-tail Student's *t*-test and represented as the mean ± SEM: $^*p < 0.05$. $n = 4$–5 independent experiments.

regenerate their axons. By itself, this observation deserves serious consideration in light of a DMD pathology, since eventual damages to muscle-innervating autonomic neurons in DMD patients could end up in impaired axon recovery and neuron survival, as well as increased autonomic dysfunctions.

However, in this study, the results obtained by the *in vitro* axotomy experiments with microfluidic chambers, in which targets are absent and the only variable is the presence of different NGF concentrations in the culture medium (either 10 ng/ml or 50 ng/ml), indicate that neuronal intrinsic damages in dystrophic mice are by themselves sufficient for reducing early regeneration capabilities. As a matter of fact, axon regeneration of *mdx* mouse neurons is significantly reduced, compared to wild type, in the presence of 10 ng/ml NGF, confirming that, among the possible neuronal alterations determined by lack of Dp427, sensitivity to NGF is a prominent one. NGF concentration could be a limiting factor also *in vivo*; indeed, the iris is a much poorer producer of NGF compared to the SbGl, the tissue from which this trophic factor is normally purified. To confirm this, when 50 ng/ml NGF were used, the regenerative performance of regenerating *mdx* mouse neurons increased, similarly to the SbGl re-innervation described by the experiments *in vivo*.

Another aspect of *in vitro* axotomy experiments was the morphological characteristics of the growth cones. As described, terminal axons were mostly bulbous in shape, filled with tangles of microtubules, which were significantly larger in *mdx* mouse neuron culture compared

Table 2
Coexistence indexes of TrkA with β-DG and β-DB in wild type and *mdx* mouse SCG neurons.

	Pearson's coefficient	Manders' coefficient TrkA/β-DG	Manders' coefficient β-DG/TrkA	Pearson's coefficient	Manders' coefficient TrkA/β-DB	Manders' coefficient β-DB/TrkA
WT	0.60 ± 0.07	0.46 ± 0.05	0.93 ± 0.01	0.50 ± 0.03	0.65 ± 0.04	0.90 ± 0.008*
mdx	0.72 ± 0.05	0.35 ± 0.04	0.90 ± 0.02	0.56 ± 0.03	0.65 ± 0.04	0.83 ± 0.02

The Pearson's correlation coefficient describes the relationship between the pixel intensities of the two channels (*i.e.* green and red) by linear correlation. This correlation varies between +1 and −1, where 1 corresponds to a perfect linear correlation and −1 corresponds to a perfect inverse correlation. Within the correlation range: values between 0 and 0.3 represent a weak correlation, those between 0.3 and 0.7 a moderate correlation, and those >0.7 a strong correlation. Manders' colocalization coefficient indicates the proportion of signal of one channel overlapping with the signal of another channel. Values <0.5 indicate absence of overlapping; values >0.5 indicate overlapping between channels. Values are expressed as the mean of 4 independent experiments ± SEM.

* $p < 0.006$ by the Student's *t*-test.

to wild type in the presence of 10 ng/ml NGF. This difference was attenuated with the 50 ng/ml NGF, a concentration at which growth cone of both genotypes enlarged significantly. Growth cone plasticity requires intense and tightly regulated mechanisms of microtubule assembly and disassembly, and active interactions with F-actin bundles. Alterations in actin-microtubule coupling causes growth cone arrest and a characteristic microtubule looping, which ends up in growth cone arrest and enlargement (reviewed by Cammarata et al., 2016; Dent et al., 1999; Dent and Kalil, 2001). In NGF-dependent neurons, these mechanisms are ruled by activation of the PI3K-Akt and Erk1/2 signaling at the growth cone (Markus et al., 2002a; Zhou et al., 2004), common also to other trophic factors (reviewed in Markus et al., 2002b). Reduction in local growth cone signaling also prevents growth cone regeneration and induces the formation of large "retraction bulbs", engulfed of microtubules, which extend in various directions, including the retrograde one (reviewed in Bradke et al., 2012). Therefore, in our experimental model, a possible reduction in the TrkA-NGF signaling in *mdx* mouse neurons, compared to wild type, could reduce cytoskeleton dynamics at the axon terminal, at least in the presence of 10 ng/ml NGF. This would slow down neuritic advancement and generate large paused growth cones. An increase in growth cone size correlated with a decrease in neurite growth rate has also been demonstrated in *Aplysia* (Ren and Suter, 2016), underlying a common mechanism.

A similar behavior was also observed for *de novo* neurite outgrowth. In line with our hypothesis, both number of principal neurites and total neuritic length were significantly reduced in *mdx* mouse neurons, compared to wild type, at all NGF concentrations used. This indicates that fundamental NGF-dependent processes, as axon growth and growth cone plasticity, are affected by lack of Dp427. This was successfully confirmed by the live imaging studies, performed in the presence of 10 ng/ml of NGF, in which *mdx* mouse neuron axons spent more time in retracting and pausing, rather than advancing, with respect to the wild type, strongly suggesting once more that these types of alterations could be ascribed to a reduced NGF-TrkA-dependent control of cytoskeletal dynamics at the growth cone. Analyzing βIII-tubulin immunofluorescence in the growth cone of neurons grown for 5 h in the presence of either 10 or 50 ng/ml NGF we again observed a sort of growth cone enlargement and frequent microtubule derangement in *mdx* mouse neurons.

Interestingly, axonal branching did not appear to be influenced by NGF culturing conditions, as the only concentration at which *mdx* mouse neurons branched significantly less than wild type was the 1 ng/ml. This concentration was also the only one affecting the capability of initiating new neurites by *mdx* mouse neurons. NGF has been reported as pivotal in axon branching of sensory neurons through a local PI3K-Akt pathway (Gallo and Letourneau, 1998, 2000; Ketschek and Gallo, 2010; Spillane et al., 2012; Ketschek et al., 2015); however, the dependence of these neurons from NGF is different compared to SCG. In addition, although formation of an axon branch, or of a new neurite, is substantially characterized by the same cytoskeletal dynamics reported for axonal growth, velocity of these processes could be greatly different: growth cone plasticity in axonal growth is a continuously ongoing process with a fast dynamics, while axonal branching and neuritic emission require an initiation of cytoskeletal rearrangement, characterized by cycles of microtubule depolymerization, re-location and protrusion (reviewed in Kalil and Dent, 2014 and Pacheco and Gallo, 2016). Therefore, we may hypothesize that a process slower than axon growth could allow *mdx* mouse neurons to compensate for their reduced NGF sensitivity and behave similarly to wild type. In addition, an interesting paper by Higuchi et al. (2003) on NGF-treated PC12 cells reported that the PI3K-Akt signaling suppresses, instead of favoring, neurite branch formation, suggesting that more studies are needed to explore this aspect.

To investigate how the signaling downstream the NGF-TrkA coupling could be eventually affected in *mdx* mouse neurons, we used the same culturing conditions (5 h) in the presence of either 10 ng/ml or 50 ng/ml NGF. Protein level analysis of phosphorylated (activated) and non-phosphorylated TrkA receptor and of components of its two major local intracellular signaling, *i.e.* PI3K-Akt and Erk1/2, gave interesting results. Undoubtedly, lower concentrations of NGF engage less TrkA receptor at the cell surface of *mdx* mouse neurons, with a consequent decrease in both intracellular signaling pathways. Since no changes in total non-phosphorylated TrkA proteins was observed, we suggest that this reduction could stem from inefficient stabilization of the receptor at the plasma membrane, indirectly pivoted by the lack of dystrophin. This would affect the signaling responsible for cytoskeletal rearrangement, functional for growth cone advancement and axon elongation. Supporting this hypothesis is the description, in *Drosophila* eye, of a tripartite functional link established between dystrophin/dystroglycan, a neuro-specific receptor kinase inserted within the plasma membrane and intracellular proteins involved in cytoskeletal remodeling (Marrone et al., 2011). Another interesting aspect is that when the concentration of available NGF increases, no differences were observed in term of TrkA phosphorylation, comforting the hypothesis that the more NGF is around the more efficiently TrkA receptor in dystrophic neurons are able to bind it. However, looking at the downstream signaling, only the PI3K apparently benefitted from this situation, as both phosphorylated and non-phosphorylated protein levels increased significantly compared to wild type neurons. Levels of *p*Akt and *p*Erk1/2, instead, remained significantly lower compared to wild type, suggesting that some mechanism within the signaling downstream TrkA phosphorylation is also affected by the lack of Dp427.

4.2. Dp427 and NGF signaling: where is the link?

A direct link between TrkA receptors and the dystrophin/DGC has never been described, but indirect connections can be envisioned. One hypothesis is that, without Dp427, clusters of TrkA receptors could be less stabilized in the plasma membrane, *i.e.* receptors dimerize less efficiently upon NGF arrival and/or remain in the membrane for shorter times compared to wild type. As a consequence, receptor phosphorylation and intracellular signaling would be reduced. In fact, NGF-induced axon growth is potentiated by TrkA receptor stabilization (Song and Yoo, 2011) and, in turn, NGF stimulation increases TrkA receptor aggregation into lipid rafts (Limpert et al., 2007; Zweifel et al., 2005). These are plasma membrane domains enriched in caveolins, a class of

proteins, which interacts directly with β-DG (Sharma et al., 2010), the central protein of the DGC (Davies and Nowak, 2006) and scaffold for signaling proteins (Cavaldesi et al., 1999; Grozdanovic and Baumgarten, 1999; Spence et al., 2004; Davies and Nowak, 2006). It has been demonstrated that the absence of Dp427 in *mdx* mice and dystrophic golden retriever dogs reduces protein levels of both β-DG and caveolin-1 in airway smooth muscle cells, weakening the ECM-actin cytoskeleton link. This, in turn, de-regulates the intracellular signals (PI3K/Akt1) that are important for smooth muscle cell specification (Sharma et al., 2014). Similarly, in our experimental model, stabilization of TrkA may rely on a proper DGC/caveolin association within lipid rafts and/or proper DGC/ECM connection. Quantitative analysis of TrkA, β-DG and β-DB immunopositive puncta at the growth cone show a similar number of TrkA-positive puncta/μm^2 between the two genotypes, and an expected significant reduction in β-DG and β-DB puncta in *mdx* mouse neurons compared to wild type. Part of the TrkA receptor coexists with both proteins, being the first demonstration that TrkA receptors may have a link with the Dp427/DGC in sympathetic neurons. However, no significant differences were observed between the mean PCC calculated at the growth cones of wild type and *mdx* mouse neurons. This suggests that, although β-DG and β-DB are reduced in *mdx* mice, (this paper; Zaccaria et al., 2000; Sharma et al., 2014) correlation among the three proteins within the same cellular domain does not change perceptibly. What could change, instead, are the time of permanence of TrkA into the plasma membrane (insertion *versus* removal), and efficiency in both its clustering within lipid rafts upon NGF arrival and intracellular signaling. As expected, the measured MCC indicates that at growth cones not all TrkA receptors coexist with β-DG and β-DB. However, in *mdx* mice, the fraction of β-DB coexisting at the same cellular domains with TrkA is significantly lower compared to wild type, suggesting a reduction in the proportion of DGC indirectly "associated" to TrkA. A similar trend is observed for the fraction β-DG/TrkA, although this difference does not reach significance, possibly because a lower efficiency of labeling of the anti-β-DG antibody compared to that of β-DB. Another aspect to be considered is the demonstration, by two hybrid system, pull down experiments and immunolocalization, of a physical interaction between β-DG and the mitogen-activated protein (MAP) kinase 2 (MEK2), which is upstream to ERK1/2 that, in turn, could be another interactor of β-DG (at least in fibroblasts) (Spence et al., 2004). Therefore, β-DG may play a multifunctional role as adaptor or scaffold for the ERK-MAP kinase cascade. This could also explain why, even when concentrations of available NGF are such to eliminate the difference in *p*TrkA levels between wild type and dystrophic neurons, the downstream signaling remains significantly reduced and may be responsible for the observed lower performance in neurite elongation, even in the presence of 100 ng/ml NGF in the culture medium.

In *mdx* mice, destabilization of the tripartite actin/DGC/ECM cross-bridge could also interfere with cytoskeletal dynamics in terminal axons. The extracellular side of the DGC binds to different proteins, the main one of which is laminin (Davies and Nowak, 2006). In the PNS, laminin strongly influences axonal growth (Tonge et al., 1997) and regeneration (Chen et al., 2007) by binding the monoganglioside GM1 localized into TrkA-containing lipid rafts (Ichikawa et al., 2009). Inside cells, Dp427 binds to both microtubules (Prins et al., 2009) and actin (Blake et al., 2002; Davies and Nowak, 2006), modifying its flexibility and creating a strong and resilient network (Prochniewicz et al., 2009). Although these data refer to skeletal muscles, or to *in vitro* studies, we can envisage a role of Dp427 in cytoskeletal dynamics also in neurons, both at growth cones and along axons. In SCG neurons, microtubules bind to TrkA receptors and are specifically attracted into lipid rafts by NGF signaling (Pryor et al., 2012), identifying these membrane domains as central for axon growth and guidance (Kamiguchi, 2006). On these terms, the association at lipid rafts of Dp427/DGC, ECM, caveolins, actin, microtubules and NGF/TrkA receptors appears multifaceted and deserves a deeper analysis.

4.3. Axon growth and regeneration: a more complex picture

We have previously demonstrated, in rat and mouse SCG, that Dp427/DGC is directly implicated in the post-synaptic stabilization of α3,β2/β4-containing nicotinic acetylcholine receptors (nAChR) (Zaccaria et al., 1998; Zaccaria et al., 2000) and that, in *mdx* mice, both their membrane localization (Zaccaria et al., 2000) and activity (Di Angelantonio et al., 2010) are reduced. Other studies report that electrically active neurons have enhanced axonal growth compared to silent neurons, promoted by a higher sensitivity to extracellular cues as a consequence of increased insertion into membrane of their specific receptors (Meyer-Franke et al., 1998; Goldberg et al., 2002). Similarly, injured neurons enhance axonal re-generation when electrically stimulated (Al-Majed et al., 2000; Brushart et al., 2005). Moreover, TrkA/NGF signaling endosomes from axon terminals control synaptic assembly on SCG neuron somato-dendritic compartments (Huang et al., 1999; Harrington and Ginty, 2013) and, in turn, NGF expression by targets depends on sympathetic neuron activity (Calinescu et al., 2011). Therefore, we could consider another aspect additional to a direct Dp427/nAChRs mechanical link, *i.e.* less sensitivity to NGF in *mdx* mouse neurons may contribute to reduce nAChR membrane expression and activity. In turn, a decrease in cholinergic activity could de-regulate NGF production by target tissues. Although in the SbGl this may not represent a problem, due to the large amount of mature NGF produced, in the iris or other types of targets it may play some role.

In conclusion, our data identify a role for dystrophin in NGF-dependent axon growth and regeneration. Although the dynamical characteristics to be considered are multiple and intermingled, the main idea is that dystrophic neurons are less sensitive to NGF compared to wild type. Due to the determinant role played by NGF in CNS and PNS development and differentiation, these aspects may require serious consideration when studying neural alterations associated with DMD.

Supplementary data to this article can be found online at http://dx.doi.org/10.1016/j.mcn.2017.01.006.

Acknowledgments

The authors wish to thank Prof. Paola Paggi, friend and mentor, for her unique and valuable support from experimental planning to critical discussion of the data. This work has been funded by, Ricerche Universitarie 2011 (C26A11CC9E), 2015 (C26A15PJLW) and 2016 (C26A15PJLW), and Agenzia Spaziale Italiana (ASI) (I/R/165/02) (MEDS); Ricerche Universitarie 2012 (C26N12BZ5K) and 2014 (C26N14FXN7) (IP). LL was recipient of an EMBO short-term fellowship at the Erasmus Medical Center, Rotterdam (The Netherlands).

References

Al-Majed, A.A., Neumann, C.M., Brushart, T.M., Gordon, T., 2000. Brief electrical stimulation promotes the speed and accuracy of motor axonal regeneration. J. Neurosci. 20, 2602–2608.

Anderson, J.L., Head, S.I., Rae, C., Morley, J.W., 2002. Brain function in Duchenne muscular dystrophy. Brain 125, 4–13.

Blake, D.J., Kroger, S., 2000. The neurobiology of Duchenne muscular dystrophy: learning lessons from muscle? Trends Neurosci. 23, 92–99.

Blake, D.J., Weir, A., Newey, S.E., Davies, K.E., 2002. Function and genetics of dystrophin and dystrophin-related proteins in muscle. Physiol. Rev. 82, 291–329.

Bradke, F., Fawcett, J.W., Spira, M.E., 2012. Assembly of a new growth cone after axotomy: the precursor to axon regeneration. Nat. Rev. Neurosci. 13, 183–193.

Brushart, T.M., Jari, R., Verge, V., Rohde, C., Gordon, T., 2005. Electrical stimulation restores the specificity of sensory axon regeneration. Exp. Neurol. 194, 221–229.

Calinescu, A.A., Liu, T., Wang, M.M., Borjigin, J., 2011. Transsynaptic activity-dependent regulation of axon branching and neurotrophin expression *in vivo*. J. Neurosci. 31, 12708–12715.

Cammarata, G.M., Bearce, E.A., Lowery, L.A., 2016. Cytoskeletal social networking in the growth cone: how 1TIPs mediate microtubule-actin cross-linking to drive axon outgrowth and guidance. Cytoskeleton (Hoboken) 73, 461–476.

Cavaldesi, M., Macchia, G., Barca, S., Defilippi, P., Tarone, G., Petrucci, T.C., 1999. Association of the dystroglycan complex isolated from bovine brain synaptosomes with proteins involved in signal transduction. J. Neurochem. 72, 1648–1655.

Chelly, J., Montarras, D., Pinset, C., Berwald-Netter, Y., Kaplan, J.C., Khan, A., 1990. Quantitative estimation of minor mRNAs by cDNA-polymerase chain reaction. Application to dystrophin mRNA in cultured myogenic and brain cells. Eur. J. Biochem. 187, 691–698.

Chen, Z.L., Yu, W.M., Strickland, S., 2007. Peripheral regeneration. Annu. Rev. Neurosci. 30, 209–233.

Cyrulnik, S.E., Hintoon, V.J., 2008. Duchenne muscular dystrophy: a cerebellar disorder. Neurosci. Biobehav. Rev. 32, 486–496.

Davies, K.E., Nowak, K.J., 2006. Molecular mechanism of muscular dystrophies: old and new players. Nat. Rev. Mol. Cell Biol. 7, 762–773.

De Stefano, M.E., Zaccaria, M.L., Cavaldesi, M., Petrucci, T.C., Medori, R., Paggi, P., 1997. Dystrophin and its isoforms in a sympathetic ganglion of normal and dystrophic *mdx* mice: immunolocalization by electron microscopy and biochemical characterization. Neuroscience 80, 613–624.

De Stefano, M.E., Leone, L., Lombardi, L., Paggi, P., 2005. Lack of dystrophin leads to the selective loss of superior cervical ganglion neurons projecting to muscular targets in genetically dystrophic *mdx* mice. Neurobiol. Dis. 20, 929–942.

Dent, E.W., Kalil, K., 2001. Axon branching requires interactions between dynamic microtubules and actin filaments. J. Neurosci. 21, 9757–9769.

Dent, E.W., Callaway, J.L., Szebenyi, G., Baas, P.W., Kalil, K., 1999. Reorganization and movement of microtubules in axonal growth cones and developing interstitial branches. J. Neurosci. 19, 8894–8908.

Di Angelantonio, S., De Stefano, M.E., Piccioni, A., Lombardi, L., Gotti, C., Paggi, P., 2010. Lack of dystrophin functionally affects α3β2/β4-nicotinic acetylcholine receptors in sympathetic neurons of dystrophic *mdx* mice. Neurobiol. Dis. 41, 528–537.

Dunn, C.W., Kamocka, M.M., McDonald, J.H., 2011. A practical guide to evaluating colocalization in biological microscopy. Am. J. Phys. Cell Physiol. 300, C723–C742.

Gallo, G., Letourneau, P.C., 1998. Localized sources of neurotrophins initiate axon collateral sprouting. J. Neurosci. 18, 5403–5414.

Gallo, G., Letourneau, P.C., 2000. Neurotrophins and the dynamic regulation of the neuronal cytoskeleton. J. Neurobiol. 44, 159–173.

Glebova, N.O., Ginty, D.D., 2004. Heterogeneous requirement of NGF for sympathetic target innervation *in vivo*. J. Neurosci. 24, 743-751.

Glebova, N.O., Ginty, D.D., 2005. Growth and survival signals controlling sympathetic nervous system development. Annu. Rev. Neurosci. 28, 191–222.

Goldberg, J.L., Espinosa, J.S., Xu, Y., Davidson, N., Kovacs, G.T., Barres, B.A., 2002. Retinal ganglion cells do not extend axons by default: promotion by neurotrophic signaling and electrical activity. Neuron 33, 689–702.

Grozdanovic, Z., Baumgarten, H.G., 1999. Nitric oxide synthase in skeletal muscle fibers: a signaling component of the dystrophin-glycoprotein complex. Histol. Histopathol. 14, 243–256.

Harrington, A.W., Ginty, D.D., 2013. Long-distance retrograde neurotrophic factor signalling in neurons. Nat. Rev. Neurosci. 14, 177–187.

Higuchi, M., Onishi, K., Masuyama, N., Gotoh, Y., 2003. The phosphatidylinositol-3 kinase (PI3K)-Akt pathway suppresses neurite branch formation in NGF-treated PC12 cells. Genes Cells 8, 657–669.

Huang, C., Zhou, J., Feng, A.K., Lynch, C.C., Klumperman, J., DeArmond, S.J., Mobley, W.C., 1999. Nerve growth factor signaling in caveolae-like domains at the plasma membrane. J. Biol. Chem. 274, 36707–36714.

Ichikawa, N., Iwabuchi, K., Kurihara, H., Ishii, K., Kobayashi, T., Sasaki, T., Hattori, N., Mizuno, Y., Hozumi, K., Yamada, Y., Arikawa-Hirasawa, E., 2009. Binding of laminin-1 to monoganglioside GM1 in lipid rafts is crucial for neurite outgrowth. J. Cell Sci. 122, 289–299.

Jagadha, V., Becker, L.E., 1988. Brain morphology in Duchenne muscular dystrophy: a Golgi study. Pediatr. Neurol. 4, 87–92.

Kalil, K., Dent, E.W., 2014. Branch management: mechanisms of axon branching in the developing vertebrate CNS. Nat. Rev. Neurosci. 15, 7–18.

Kamiguchi, H., 2006. The region-specific activities of lipid rafts during axon growth and guidance. J. Neurochem. 98, 330–335.

Ketschek, A., Gallo, G., 2010. Nerve growth factor induces axonal filopodia through localized microdomains of phosphoinositide 3-kinase activity that drive the formation of cytoskeletal precursors to filopodia. J. Neurosci. 30, 12185–12197.

Ketschek, A., Jones, S., Spillane, M., Korobova, F., Svitkina, T., Gallo, G., 2015. Nerve growth factor promotes reorganization of the axonal microtubule array at sites of axon collateral branching. Dev. Neurobiol. 75, 1441–1461.

Kim, H.S., Yumkham, S., Kim, S.H., Yea, K., Shin, Y.C., Ryu, S.H., Suh, P.G., 2006. Secretin induces neurite outgrowth of PC12 through camp-mitogen-activated protein kinase pathway. Exp. Mol. Med. 38, 85–93.

Koenig, M., Hoffman, E.P., Bertelson, C.J., Monaco, A.P., Feener, C., Kunkel, L.M., 1987. Complete cloning of the Duchenne muscular dystrophy (DMD) cDNA and preliminary genomic organization of the DMD gene in normal and affected individuals. Cell 50, 509–517.

Kohn, J., Aloyz, R.S., Toma, J.G., Haak-Frendscho, M., Miller, F.D., 1999. Functionally antagonistic interactions between the TrkA and p75 neurotrophin receptors regulate sympathetic neuron growth and target innervation. J. Neurosci. 19, 5393–5408.

Licursi, V., Caiello, I., Lombardi, L., De Stefano, M.E., Negri, R., Paggi, P., 2012. Lack of dystrophin in *mdx* mice modulates the expression of genes involved in neuron survival and differentiation. Eur. J. Neurosci. 35, 691–701.

Limpert, A.S., Karlo, J.C., Landreth, G.E., 2007. Nerve growth factor stimulates the concentration of TrkA within lipid rafts and extracellular signal-regulated kinase activation through c-Cbl-associated protein. Mol. Cell. Biol. 27, 5686–5698.

Lombardi, L., De Stefano, M.E., Paggi, P., 2008. Components of the NGF signaling complex are altered in *mdx* mouse superior cervical ganglion and its target organs. Neurobiol. Dis. 32, 402–411.

Markus, A., Zhong, J., Snider, W.D., 2002a. Raf and Akt mediate distinct aspects of sensory axon growth. Neuron 35, 65–76.

Markus, A., Patel, T.D., Snider, W.D., 2002b. Neurotrophic factors and axonal growth. Curr. Opin. Neurobiol. 12, 523–531.

Marrone, A.K., Kucherenko, M.M., Rishko, V.M., Shcherbata, H.R., 2011. New dystrophin/dystroglycan interactors control neuron behavior in *Drosophila* eye. BMC Neurosci. 1, 93.

Mehler, M.F., 2000. Brain dystrophin, neurogenetics and mental retardation. Brain Res. Rev. 32, 277–307.

Meyer-Franke, A., Wilkinson, G.A., Kruttgen, A., Hu, M., Munro, E., Hanson Jr., M.G., Reichardt, L.F., Barres, B.A., 1998. Depolarization and camp elevation rapidly recruit TrkB to the plasma membrane of CNS neurons. Neuron 21, 681–693.

Myers, K.A., Baas, P.W., 2007. Kinesin-5 regulates the growth of the axon by acting as a brake on its microtubule array. J. Cell Biol. 178, 1081–1091.

Noël, G., Tham, D.K., Moukhles, H., 2009. Interdependence of laminin-mediated clustering of lipid rafts and the dystrophin complex in astrocytes. J. Biol. Chem. 284, 19694–19704.

Pacheco, A., Gallo, G., 2016. Actin filament-microtubule interactions in axon initiation and branching. Brain Res. Bull. 126, 300–310.

Park, J.W., Vahidi, B., Taylor, A.M., Rhee, S.W., Jeon, N.L., 2006. Microfluidic culture platform for neuroscience research. Nat. Protoc. 1, 2128–2136.

Pilgram, G.S., Potikanond, S., Baines, R.A., Fradkin, L.G., Noordermeer, J.N., 2010. The roles of the dystrophin-associated glycoprotein complex at the synapse. Mol. Neurobiol. 41, 1–21.

Prins, K.W., Humston, J.L., Mehta, A., Tate, V., Ralston, E., Ervasti, J.M., 2009. Dystrophin is a microtubule-associated protein. J. Cell Biol. 186, 363–369.

Prochniewicz, E., Henderson, D., Ervasti, J.M., Thomas, D.D., 2009. Dystrophin and utrophin have distinct effects on the structural dynamics of actin. Proc. Natl. Acad. Sci. 106, 7822–7827.

Pryor, S., McCaffrey, G., Young, L.R., Grimes, M.L., 2012. NGF causes TrkA to specifically attract microtubules to lipid rafts. PLoS One 7, e35163.

Reichardt, L.F., 2006. Neurotrophin-regulated signalling pathways. Philos. Trans. R. Soc. Lond. Ser. B Biol. Sci. 361, 1545–1564.

Ren, Y., Suter, D.M., 2016. Increase in growth cone size correlates with decrease in neurite growth rate. Neural Plast. 2016, 34979010.

Sharma, N., Deppmann, C.D., Harrington, A.W., St. Hillaire, C., Chen, Z.-Y., Lee, F.S., Ginty, D., 2010. Long-distance control of synapse assembly by target-derived NGF. Neuron 67, 422–434.

Sharma, P., Basu, S., Mitchell, R.W., Stelmack, G.L., Anderson, J.E., Halayko, A.J., 2014. Role of dystrophin in airway smooth muscle phenotype, contraction and lung function. PLoS One 9, e102737.

Song, E.J., Yoo, Y.S., 2011. Nerve growth factor-induced neurite outgrowth is potentiated by stabilization of TrkA receptors. BMB Rep. 44, 182–186.

Spence, H.J., Dhillon, A.S., James, M., Winder, S.J., 2004. Dystroglycan, a scaffold for the ERK-MAP kinase cascade. EMBO Rep. 5, 484–489.

Spillane, M., Ketschek, A., Donnelly, C.J., Pacheco, A., Twiss, J.L., Gallo, G., 2012. Nerve growth factor-induced formation of axonal filopodia and collateral branches involves the intra-axonal synthesis of regulators of the actin-nucleating Arp2/3 complex. J. Neurosci. 32, 17671–17689.

Taylor, A.M., Blurton-Jones, M., Rhee, S.W., Cribbs, D.H., Cotman, C.W., Jeon, N.L., 2005. A microfluidic culture platform for CNS axonal injury, regeneration and transport. Nat. Methods 2, 599–605.

Tonge, D.A., Golding, J.P., Edbladh, M., Kroon, M., Ekstrom, P.E., Edstrom, A., 1997. Effects of extracellular matrix components on axonal outgrowth from peripheral nerves of adult animals *in vitro*. Exp. Neurol. 146, 81–90.

Tsui-Pierchala, B.A., Ginty, D.D., 1999. Characterization of an NGF-P-TrkA retrograde-signaling complex and age-dependent regulation of TrkA phosphorylation in sympathetic neurons. J. Neurosci. 19, 8207–8218.

Vaillend, C., Billard, J.-M., Laroche, S., 2004. Impaired long-term spatial and recognition memory and enhanced CA1 hippocampal LTP in the dystrophin-deficient Dmd^{mdx} *mouse*. Neurobiol. Dis. 17, 10–20.

Waite, A., Tinsley, C.L., Locke, M., Blake, D.J., 2009. The neurobiology of the dystrophin-associated glycoprotein complex. Ann. Med. 41, 344–359.

Wyatt, S., Davies, A.M., 1995. Regulation of nerve growth factor receptor gene expression in sympathetic neurons during development. J. Cell Biol. 130, 1435–1446.

Yotsukura, M., Sasaki, K., Kachi, E., Sasaki, A., Ishihara, T., Ishikawa, K., 1995. Circadian rhythm and variability of heart rate in Duchenne-type progressive muscular dystrophy. Am. J. Cardiol. 76, 947–951.

Zaccaria, M.L., De Stefano, M.E., Properzi, F., Gotti, C., Petrucci, T.C., Paggi, P., 1998. Disassembly of the cholinergic postsynaptic apparatus induced by axotomy in mouse sympathetic neurons: the loss of dystrophin and beta-dystroglycan immunoreactivity precedes that of the acetylcholine receptor. J. Neuropathol. Exp. Neurol. 57, 768–779.

Zaccaria, M.L., De Stefano, M.E., Gotti, C., Petrucci, T.C., Paggi, P., 2000. Selective reduction in the nicotinic acetylcholine receptor and dystroglycan at the postsynaptic apparatus of mdx mouse superior cervical ganglion. J. Neuropathol. Exp. Neurol. 59, 103–112.

Zhou, F.-Q., Zhou, J., Dedhar, S., Wu, Y.-H., Snider, W.D., 2004. NGF-induced axon growth is mediated by localized inactivation of GSK-3 and functions of the microtubule plus end binding protein APC. Neuron 42, 897–912.

Zweifel, L.S., Kuruvulla, R., Ginty, D.D., 2005. Functions and mechanisms of retrograde neurotrophin signalling. Nat. Rev. Neurosci. 6, 15–25.